Chapter 3

DYNAMICAL TREATMENT OF THE FLUX EXPULSION (FBE)

3.1 Introduction

The central concept in the flux expulsion scenario for the magnetic evolution of neutron stars discussed in the previous chapter is the idea of the interpinning of the fluxoids and the vortices. This is however an issue which is least explored so far. Pinning of the quantized magnetic fluxoids to lattice defects and impurities in the case of type-II laboratory superconductors is a key issue in explaining their magnetic properties. The pinning is necessary in order for the so-called "hard" superconductors to be able to support large supercurrents and magnetic fields, as it prevents the fluxoids from moving freely under the existing Lorentz forces acting on them (Anderson & Kim 1964). Also, for the laboratory case of rotating superfluid ^{4}He pinning of the vortex lines to the surface of the container results in new properties for the spin behavior of the fluid as has been observed experimentally (see review by Sonin 1987). Pinning of neutron superfluid vortices to nuclei in the crust of neutron stars has been invoked by Anderson & Itoh (1975) for explaining the observed jumps in the rotation rates of some radio pulsars and the slow relaxations after such events, ie. glitches (see chapter 4). Less clear is the interaction and pinning between the two different families of vortex lines

coexisting in the interior of a neutron star (see § 1.2 and § 2.2.1).

In the original model of spin-down-induced flux expulsion (the SIF model) which was adopted in the previous studies referred to earlier, the pinning was suggested to result in a expulsion of the magnetic flux at a rate equal to the spin-down rate of the star (Srinivasan et al. 1990). The fluxoids were therefore assumed to be continually pulled out of the stellar core along with the outward moving vortices as the star spins down. However, due to the existing resistance against the motion of fluxoids and vortices and given the finite strength of the interaction energy associated with any assumed pinning mechanism the fluxoids and the vortices might be expected to move with different velocities, while "cutting" or "creeping" through each other. *A more refined treatment of the flux expulsion out of the core of neutron stars would hence require the dynamics of the fluxoid motion to be considered independently.*

In the following, we discuss the various forces which act on the flwoids in the interior of a neutron star, including a force due to their pinning interaction with the moving neutron vortices. Other forces which we take into account are

- viscous drag force due to magnetic scattering of electrons,
- buoyancy force, and
- curvature force.

The velocity of the outward motion of the fluzoids is thus determined, for a given steady-state spin-down rate of the star, from a solution of the Magnus equation requiring a balance of the different forces acting radially on a unit length of a fluxoid. The derived radial velocity of the flwoids at the core-crust boundary would then determine the rate of the flux expulsion out of the core. The original SIF model assumes that the velocity of the fluxoids is always equal to that of the neutron vortices. Our attempt is analogous to that of Ding, Cheng & Chau (1993) in their study of the field evolution of single normal pulsars. The main objective of the present work is however to investigate the results of such a treatment of the flux expulsion scenario for the magnetic evolution of *binary pulsars* for which the spin-down history of the neutron star is expected to be different

than that of the single pulsars considered by Ding et al. (1993). Furthermore, we have explored other possibilities different than those assumed by Ding et al. (1993) about the nature and magnitudes of the effective forces acting on the fluxoids. Alternative models for calculating the rate of the magnetic flux expulsion in neutron stars are thus realized. Predictions of the models for the magnetic evolution of binary as well as single pulsars are then compared and tested against the available observational data. We shall also compare the results of these more detailed studies of the flux expulsion scenario with those obtained from the much simpler approach adopted in the SIF model. This is particularly useful because the SIF model has been already shown to produce acceptable and useful resluts, as mentioned earlier.

3.2 Dynamics of Fluxoids

3.2.1 Neutron Superfluid Vortices

In the steady-state, the neutron vortices in the interior of a rotating magnetized neutron star are expected to be co-rotating at a given rate Ω with the charged component of the star, including the lattice of the proton fluxoids (Sauls 1989). The plasma in the core has been shown to be coupled to the crust over time scales $\lesssim 10$ s, for the case of non-superconducting protons (Easson 1979). The coupling mechanism is thought to be via the formation of Ekman boundary layer at the core-crust interface as in ordinary fluids (see eg. Greenspan 1969). In this process the boundary layer at the top and bottom of the fluid (for an assumed idealized cylindrical geometry) serves to bring the fluid to the new rotation rate of the container via formation of a radial secondary flow toward and away from the axis. Two types of boundary layers are possible in the case of core fluid of a neutron star, depending on whether the magnetic field or the plasma viscosity has the dominant effect. However for an assumed type-I1 superconductor plasma in the core of neutron stars most of the plasma lies in regions where there is no magnetic field and hence the coupling time scale in this case might be expected to be different than the above case. Although model calculations for the superconductor case have

not been yet carried out, similar coupling time scales ($\sim$ 10 s) have been suggested by Alpar, Langer & Sauls (1984) for this case, too, on the following grounds. They argue that viscosity due to electron-electron scattering alone indicates an Ekman time scale of 1–10 s, and fluxoids are coupled to the electron gas on time scales of 10^{-14} s due to the magnetic scattering. Proton fluid outside the fluxoids on the other hand should respond to the motion of electrons through an adjustment of the supercurrent in accord with the new condition of the electron fluid motion. The latter process is argued to proceed at the speed of light propagation giving a time scale of 10^{-4} s. *Thus the coupling time scale between the crust and the plasma in the core of a neutron star for the case of superconducting protons is decided by the* electron fluid viscosity as *in the the case of normal plasma. The time scale for relaxation of any relative velocity between the plasma and the neutron vortices, on the other hand, due to scattering of electrons off magnetic field of the vortices is* $\lesssim 20$ *s* (Alpar et al. 1984b).

However, for a star which is spinning down at a rate $\dot{\Omega}$ the rotation of the vortices would maintain a constant lag w behind the neutron superfluid bulk matter. The latter is assumed to be rotating uniformly with a rate Ω_s so that $w \equiv \Omega_s - \Omega > 0$. For a given superfluid spin-down rate $\dot{\Omega}_s$ (which, in the steady state, will be equal to the spin-down rate of the rest of the star vis. $\dot{\Omega}$) the corresponding velocity of the vortex outward motion v_n at the core boundary, is given by

$$\begin{aligned} v_n &= -\frac{R_c}{2}\frac{\dot{\Omega}}{\Omega_s} \\ &\approx -\frac{R_c}{2}\frac{\dot{\Omega}}{\Omega} \end{aligned} \tag{3.1}$$

where we have approximated Ω_s by R, and R_c is the radius of the core of a neutron star. Substituting for $R_c = 9 \times 10^5$ cm, and $\frac{\dot{\Omega}}{\Omega_s} = \frac{\dot{P}_s}{P_s}$ where P_s and $\dot{P}_s$ are spin period and its time derivative in units of seconds and s s^{-1}, respectively, result in

$$v_n = 1.59 \times 10^{-2} \frac{\dot{P}_{yr}}{P_s} \text{ cm s}^{-1} \tag{3.2}$$

where $\dot{P}_{yr}$ is the spin-down rate in units of s yr^{-1}.

On the other hand, the rotational lag results in an outward Magnus force on the

vortices which is responsible for the outward migration of the vortices and hence a reduction in their number density in a spinning down superfluid.

The Magnus force :

A vortex line in a rotating superfluid is expected to be carried along with the local superfluid velocity according to Kelvin's circulation theorem applied to transport of rectilinear vorticity in a 2D flow (Fetter 1976; Putterman 1979). However the superfluid may transmit a force to a vortex ***moving*** *with respect to the local fluid* which has the form of the classical Magnus force acting on a rotating cylindrical body moving through a fluid perpendicular to its axis (Batchelor 1967, p. 427). The relevance of a Magnus force for quantized vortices has been shown both in the case of a rotating neutral condensate (Hall & Vinen 1956) and also for a charged superfluid on fluxoids in a type-I1 superconductor (Nozikres & Vinen 1966). The Magnus force per unit length of a vortex is given as

$$\vec{F}_{\rm Magnus} = \rho_{\rm sf}\vec{\kappa} \times (\vec{v}_{\rm L} - \vec{v}_{\rm sf}) \qquad (3.3)$$

where $\rho_{\rm sf}$ is the superfluid density, $\vec{\kappa}$ is the vorticity of the vortex line directed along the rotation axis, and $\vec{v_{\rm sf}}$ and $\vec{v_{\rm L}}$ are the local superfluid and the vortex line velocities. Note that in the case of superconductor fluxoids $\vec{\kappa} \equiv \frac{e\vec{\phi}_0}{cm_{\rm c}}$, where $\vec{\phi}_0$ is the magnetic flux through the fluxoid and $m_{\rm c}$ is the mass of the superconducting particles (Nozikres & Vinen 1966).

The lag *w* and the resulting outward radial Magnus force on the neutron vortices in the spinning-down core superfluid are necessary in order to balance the existing viscous forces against outward motion of vortices. The latter forces are usually assumed to be mainly due to the scattering of the electrons from the magnetized cores of the neutron vortices in the interior of a neutron star (Sauls 1989). The requirement for vanishing net force on vortices is due to the usual approximation of treating vortices as massless fluid configurations (Sonin 1987). An effective mass is nevertheless attributed to a moving vortex due to an additional flow ipduced by its motion which contributes to the kinetic energy of the system. For the neutron and proton vortices in a neutron star

the effective mass per unit length of the vortex m^* is found to be equal to the mass of superfluid displaced by a unit length of the vortex, ie. $m^* = \rho_s \pi \xi^2 \sim 10^{-12}$ g, where ρ is the density and ξ is the radius of the vortex (Baym & Chandler 1983). The associated inertial force per unit length of the vortex would be extremely small ($< 10^{-33}$ dyn) for both neutron and proton vortices, compared to other forces considered, and will be neglected.

The pinning force on the neutron vortices :

On the other hand, if a fluxoid can pin on a vortex the associated pinning force on the vortex could be in principle in either radial direction (inward or outward), depending on the direction of the relative motion of the vortex and the fluxoid, and independent of the actual direction of motion of the vortices. Hence the pinning force might either contribute to the viscous forces against the outward motion of the vortices (which is the case when they are moving faster than fluxoids) or in the opposite case it could act as a "driving" force during a spin-down phase of the star (since in this case it points along the direction of motion of the vortices). The viscous force on the vortices due to the electron scattering is, however, expected to be many orders of magnitudes smaller than the pinning force even for the largest steady-state spin-down rates of interest and hence the largest possible values of v_n. The force per unit length of a vortex due to the pinning is typically expected to be $>> 10^{12}$ dyn cm^{-1}, while that of the electron scattering (Alpar & Sauls 1988) is $< 10^5$ dyn cm^{-1} (and the buoyancy force on the magnetized neutron vortices is even smaller than this; see § 3.2.3). ***The Magnus force on the vortices should be therefore balanced only by the pinning forces exerted by the fluxoids on them.*** An interesting consequence of this balance of forces on the vortices in the interior of a neutron star is that the vortices might be rotating ***faster*** than the neutron superfluid ($w < 0$) while it is ***spinning down.*** This is in contrast to the normal conditions of a superfluid spin-down phase where the vortices must be rotating slower ($w > 0$), so that the viscous force on the outward moving vortices is balanced by an outward "driving" Magnus force. In a neutron star, if the pinning force

due to the fluxoids is itself directed ***outward*** during a spin-down episode it could play the role of the "driving" force on the neutron superfluid vortices and the balancing Magnus force has to be directed inward. The conditions for a negative rotational lag $(\omega = \Omega, -\Omega < 0)$ as well as an inward Magnus force during a spin-down phase of the neutron superfluid is therefore realized when the outward motion of the fluxoids is faster than that of the vortices.

3.2.2 The Pinning Force on the Fluxoids

In any case, a pinning force of the same magnitude as, and in the opposite direction to, that exerted by the fluxoids will be also acting on them, due to the reaction of the vortices.

Throughout we will be considering the motion of the fluxoids only in the region close to the core-crust boundary. The strength of the average field of the stellar core is determined by the transport of these boundary fluxoids out of the core, and it is assumed that the rest of the fluxoids in the interior regions will adjust their positions and maintain a uniform density throughout the core. We will also neglect all the projection effects due to an inclination between the two lattices of the vortex lines and assume that all forces on the fluxoids as well as their velocities are directed radially in the magnetic equatorial plane. The Magnus force on the vortices and their outward velocities in the same region would however be co-linear with that of the fluxoids only for those vortex segments which lie close also to the spin equator of the star. The fractional size of such a region (of coincidence of the two equators) would be larger, and hence our treatment of the radial velocities and forces for the fluxoids and the vortices would be more accurate for smaller inclination angles.

It might, on the other hand, be argued that since the pinning interaction energy is independent of a displacement of a neutron vortex parallel to the fluxoid pinned to it the vortices might be able to slide along the fluxoids without producing a large scale movement of the fluxoids. It is noted that such a sliding might be realized for the vortices only in some parts of the spin equator, namely for those lying at large magnetic

latitudes. Nevertheless this possibility does not by itself violate the assumption of a radial reactive force acting on the fluxoids even in those regions where the sliding might occur. The Magnus force on a sliding vortex would have the same magnitude and direction as for the non-sliding vortices and its component in the direction perpendicular to the fluxoid has to be balanced in any case with a force due to the pinning which will exert a reaction force on the fluxoid. Furthermore, since the assumed sliding cannot be realized for all of the vortices for any assumed geometry of the lines its partial occurrence, if at all, seems to be further questionable on the account that it would result in an azimuthally non-uniform vortex density distribution. This point will be further discussed in chapter 4.

The pinning force:

Having said that the Magnus force on neutron vortices is balanced by the pinning force on them exerted by the fluxoids, we now proceed to estimate the *reaction* force felt by a unit length of a fluxoid. Equating the pinning forces communicated between the two lattices per unit volume, the pinning force *per unit length* of a fluxoid F_n can be expressed as

$$F_n = \frac{n_v}{n_f} F_M \tag{3.4}$$

where $n_v = \frac{2\Omega_s}{\kappa}$ and $n_f = \frac{B_c}{\phi_0}$ are the number densities per unit cross section areas of the vortices and the fluxoids, respectively, $\kappa = 2 \times 10^{-3} \mathrm{cm^2 s^{-1}}$ is the vorticity of a vortex line, $\phi_0 = 2 \times 10^{-7} \mathrm{G cm^2}$ is the magnetic flux carried by a fluxoid, B_c is the strength of the core field in units of G, and F_M is the Magnus force per unit length of a *neutron vortex* at the core boundary. For the relative azimuthal velocity between vortices and the neutron superfluid due to the lag w, the radial Magnus force is $F_M = \rho_s \kappa R_c \omega$, where ρ_s is the neutron superfluid density (see Eq. 3.3). Substituting in Eq. 3.4 gives

$$\begin{aligned} F_n &\approx 2\phi_0 \rho_s R_c \frac{\Omega(t)\,\omega(t)}{B_c(t)} \\ &= 5.03 \frac{(3\text{-}6}{P_s B_8} \text{ dyn cm}^{-1} \end{aligned} \tag{3.5}$$

where we have again approximated $\Omega \approx \Omega_s$, ω_{-6} is the superfluid lag w in units of 10^{-6}rad s^{-1}, $B_c = 10^8 B_8$, and $\rho_s = 2 \times 10^{14}$gcm^{-3} has been used. Note that the sign of w will determine the sign of F_n for which, as well as for the other forces discussed below, the outward direction will be reckoned as the positive sense.

The above derivation of F_n is however based on certain assumptions which need to be clarified. The total Magnus force acting continuously on dl the neutron superfluid vortices has been assumed to be communicated instantaneously to the fluxoids through the reactive pinning force on them. This need not be always true since, in general, only a small fraction of the vortices might be expected to be directly interacting with the fluxoids at any instant of time. The remaining much greater fraction of them (of the order of the ratio of a fluxoid-spacing to the size of a pinning interaction region) would, however, lie in the inter-fluxoid spacings. Also, the assumed total force on the flwoids has been divided equally among all fluxoids in spite of the fact that at any given time a majority of them would be located in the inter-vortex regions far from any pinning site. Nevertheless, the motion of the fluxoids (as well as the vortices) is further constrained due to the mutual *repulsive* forces among themselves. This would prevent them from being swept independently and requires a uniform density of lines to be maintained in the steady state. Consequently all fluxoids (whether being in an interaction region or in a free region) are forced to move always together and the force acting on some of them is shared equally among all, instantaneously. This argument fails however for the neutron vortices since for them displacements of some of them on scales of the order of a fluxoid-spacing (which is many orders of magnitudes smaller than the vortex-spacing) is not prohibited by the above constraint of the uniform density (in a different context Anderson & Kim 1964 have also remarked on this). For the same reason, any given vortex which is not interacting with a fluxoid at a given time is expected to move relative to the rest of the vortices and adjusts its position rapidly (within a distance of a fluxoid-spacing) so that it also feels the same viscous force due to the pinning with a flwoid. Therefore, in a steady-state co-moying vortex-fluxoid phase all the vortices are expected to be located within pinning interaction regions, and hence the total Magnus

force on them has to be taken into account, as in Eq. 3.5.

However, such a restriction on the vortex positions cannot be guaranteed at all times if the radial velocities of the vortices and the fluxoids are different, since the vortices have to travel through the inter-fluxoids distances as well. The effective instantaneous force per unit length of a fluxoid, F_n, during such a state is therefore smaller than that given in Eq. 3.5 and might be estimated by considering the time averaged force on the fluxoids (or equivalently the average fractional number of the vortices that are expected to be interacting with the fluxoids at any given time) which results in

$$F_n = \frac{d_P}{d_f}\left(\frac{n_v}{n_f}F_M\right) \tag{3.6}$$

where d_f is the flwcoid-spacing, and d_P is the effective size of a pinning interaction region around each fluxoid. For the assumed magnetic pinning mechanism (see below), the effectiveLondon length of the proton superconductor λ_p^* which is a characteristic length scale for the magnetic field around a neutron vortex line may be used for the size of the interaction region. Substituting for $d_f = 2.3 \times 10^{-7} B_8^{-\frac{1}{2}}$ cm, and $d_P = \lambda_p^* \sim 118$ fm in Eq. **3.6** and using Eq. 3.5 results in

$$F_n = 2.59 \times 10^{-4} \frac{\omega_{-6}}{P_s B_8^{1/2}} \text{ dyn cm}^{-1} \tag{3.7}$$

It has to be noted that for evaluating the "averaged" value of F_n as given in Eqs **3.6** and **3.7** the velocity of a vortex while it is crossing through an interaction region has been assumed to be same as that in the free space between the fluxoids; equal weights have been therefore assigned to the corresponding periods of times .

Realistically the vortices might be expected to move much faster while they are in the "free" regions than in the pinning regions because of the large difference in the effective viscous forces acting on the them in the two regions (as discussed above). As a consequence they tend to spend most of the time within the pinning zones and an almost zero weight has to be considered for the time durations when no pinning force is acting on a vortex. Consequently the same estimate for F_n as in Eq. 3.5 might be used even for the cases when the fluxoids and the vortices move with different velocities and cross through each other.

Each of the above derivations for F_n as given in Eq. 3.5 and Eq. 3.7 might be expected to represent a better approximation depending on the assumed behavior of the neutron vortices regarding the creeping of the different pinned segments of a vortex. If each pinned segment of a vortex could move independently (over the length scales of about a fluxoid-spacing) then the above argument to justify Eq. **3.4** (and Eq. 3.5) for the creeping phases applies. In contrast, for a vortex line of infinite rigidity the whole line moves always as a single piece and F_n as in Eq. 3.6 (and Eq. 3.7) would be appropriate. We will adopt both the above estimates for F_n during phases when $v_n \neq v_p$ in alternative models which we explore.

The " critical lag":

The magnitude of the force which is exerted by a vortex on a fluxoid, and vice versa, *at each intersection* (and hence F_n) is limited by a maximum value f_P corresponding to the given strength of the pinning energy E_P and the finite length scale of the interaction, namely $E_P = f_P d_P$. The Magnus force on the vortices which is assumed to be balanced by the pinning force cannot therefore exceed a corresponding limit which in turn implies also a maximum absolute value for the lag w (to recall $w = \Omega_s - \Omega_L$, where Ω_s is the superfluid rotation rate and Ω_L is the rotation rate of the vortices). The maximum absolute value of the lag, the critical lag w_c may be determined by equating the Magnus force on unit length of a vortex $(\rho_s \kappa R_c \omega)$ with the maximum available pinning force per unit length of the vortex $(\frac{f_P}{d_f} \equiv \frac{E_P}{d_f d_P})$. The pinning energy, in the magnetic interaction mechanism, arises because of the difference in the free energy of a fluxoid-vortex pair whether they cross each other or not. For a fluxoid with an average field $\vec{B}_p$ and a vortex having an average field $\vec{B}_n$, the magnetic energy density when they overlap at an intersection would include a term $(2/8\pi)\vec{B}_p.\vec{B}_n$, in addition to the sum of their contributions to the energy density when they are separate, ie. $(B_p^2 + B_n^2)/8\pi$. The pinning energy per intersection may be thus estimated as $(2/8\pi)\vec{B}_p.\vec{B}_n$ times the interaction overlap volume $\sim (2\lambda_p)(\pi\lambda_p^{*2})$, which results in $E_P \sim 10^{-5}$ ergs (see Jones 1991 for a more refined derivation). Using the associated value of $d_P \sim \lambda_p^*$ for the

magnetic pinning, the maximum critical lag ω_{cr} is estimated as

$$\omega_{cr} = 1.59 \times 10^{-6} B_8^{1/2} \text{ rad s}^{-1} \tag{3.8}$$

where we have used the same expression as in Ding et al. (1993) in order for the further comparison of the results. Thus during a co-moving state where the force communicated between a vortex and a fluxoid at each pinning point is less than its maximum value, f_P, the lag might have any value within the range $-\omega_{cr} < w < w$, However when the vortices move faster or slower than the fluxoids, a constant value of $w = \omega_{cr}$ or $w = -\omega_{cr}$ will be maintained, respectively.

We note that a different estimate for the pinning energy due to the proton density perturbation gives a smaller value of $E_P \sim 5 \times 10^{-7}$ ergs. The pinning energy in this case arises due to the difference in the condensation energy between the pinned and the free configurations, which is in turn due to the change in the proton density induced by the large velocity of the neutrons close to the core of a neutron vortex. The interaction volume for this mechanism is $\sim \xi_n^2 \xi_p$, and the change in the free energy density is estimated as $n_n \frac{\Delta_p^2}{E_{F_p}^2} \frac{\Delta_n^2}{E_{F_n}^2}$, where Δ is the condensation energy gap, E_F the Fermi energy, ξ the coherence length, and n the number density; the subscripts p and n refer to protons and neutrons respectively (Sauls 1989). Eventhough the value of the pinning energy due to the density perturbation is smaller than that of the magnetic interaction, however since the associated value of the interaction length – the London penetration depth in the latter case – is also larger by about the same ratio than for a pinning due to the density perturbation, similar values of f_P, and hence ω_{cr}, are expected for the both pinning mechanisms (Bhattacharya and Srinivasan 1991). Also, since the magnetic interaction depends on the angle between the fluxoids and the vortices at the intersection points the pinning due to the density perturbation might indeed have the dominant effect in a neutron star with a nearly parallel geometry of the vortices and fluxoids.

In this rather long subsection we have argued that the effective value of the pinning force on the fluxoids is (not the maximum possible value f_P and is) decided by the Magnus force on the neutron vortices, which in turn is determined by the rotational

lag between the vortices and the neutron superfluid. Two alternative estimates for the pinning force were also discussed, as well as the maximum absolute value of the lag due to the finite strength of the pinning energy. In our model calculations the value of F_n as given in Eq. 3.5 will be used for a co-moving state of the fluxoids and the vortices. However for states with different velocities of the two families of lines either of the two estimates as in Eqs 3.5 and 3.7 is adopted, alternatively, in different models (see Table 1 below).

3.2.3 Other Forces on the Fluxoids

In addition to the force F_n due to the pinning with the vortices, the fluxoids in the interior of a neutron star are expected to be also subject to other forces which should be taken into account in order to determine their outward radial motion in the stellar core. We consider three force below: viscous drag force, buoyancy force, and curvature force.

The drag force:

An isolated fluxoid moving through the normal degenerate electron gas in the core of a neutron star is subject to viscous drag forces due to scattering of the electrons by the magnetic field of the fluxoid.

A simple order of magnitude calculation of the drag force due to magnetic scattering of electrons might be given based on the geometrical and dynamical considerations as follows (see also Harvey et al. 1986). Electrons in the core of a neutron star have associated de Broglie wavelengths ($\lambda/2\pi \sim 3 \times 10^{-13}$ cm) much smaller than the effective radius of a fluxoid A, $\sim 10^{-11}$ cm. Hence classical trajectories can be assigned to the electrons in their interaction with the fluxoids. The force on a unit length of a fluxoid parallel and opposite to its velocity $\vec{v_p}$ may thus be written as a product of the flux of particles ($\sim 2\lambda_p n_e v_p$) times the average change in momentum of an electron p_e being scattered through an angle θ ($\sim p_e < 1 - \cos\theta >$, where the bracket indicates averaging over all possible scattering angles). Furthermore, the gyration radius of an

electron in the field of a fluxoid $a_{H1} \sim \frac{p_e c}{eH_{c1}} \sim \frac{E_F}{eH_{c1}} \sim 10^{-9}$ cm is much larger than the radius of the fluxoid, where $H_{c1} = \frac{\phi_0}{4\pi\lambda_p^2} \ln \frac{\lambda_p}{\xi}$ is the lower critical field of the type-I1 proton superconductor which is also the value of the field within a fluxoid (see eg. de Gennes 1966, pp. 55–60), and where λ_p and ξ are the London penetration depth and the coherence length of the proton superconductor, respectively. Hence electrons are deflected through small angles of order $\theta_0 \sim \frac{\lambda_p}{a_{H1}} \sim 10^{-2}$ upon scattering at each fluxoid. Therefore the angular term $< 1 - \cos\theta > \sim 1 - \cos\theta_0 = 2\sin^2\frac{\theta_0}{2} \sim d_0^2 \sim \left(\frac{\lambda_p}{a_{H1}}\right)^2$. This will give us an estimate for the viscous drag force per unit length of a fluxoid

$$\vec{F_v} \sim -\frac{2}{\pi^2} \frac{n_e e^2 \phi_0^2}{E_F \lambda_p} \frac{\vec{v_p}}{c} \tag{3.9}$$

A more refined estimate due to Jones (1987) gives

$$\begin{aligned} \vec{F_v} &= -\frac{3\pi}{64} \frac{n_e e^2 \phi_0^2}{E_F \lambda_p} \frac{\vec{v_p}}{c} \\ &= -7.30 \text{ x } 10^7 \vec{v_p} \text{ dyn cm}^{-1} \end{aligned} \tag{3.10}$$

where n_e is the number density of the electrons, E_F is the electron Fermi energy, v_p is the velocity of the radial outward motion of the fluxoids in units of cm s^{-1}, and values of $n_e \sim 3. \text{ x } 10^{36} \text{cm}^{-3}$ and $E_F \sim 88.$ *MeV* corresponding to total core density $\rho \sim 2. \text{ x } 10^{14} \text{g cm}^{-3}$, and neutron density $n_n \sim 1.7 \text{ x } 10^{38} \text{cm}^{-3}$ have been used. Jones' derivation is based on finding the change in electron distribution function from its equilibrium isotropic form in momentum space away from a vortex due to interactibn with the field of a vortex from a solution of the Boltzman equation. The associated power dissipation due to acceleration of electrons in the induced electric field and hence the corresponding viscous force is then calculated as given above.

The expression for F_v in Eq. 3.10 is derived based on the assumption of *independent fluxoids motions*. It has been argued that this is not justified for the typical conditions in the interior of a neutron star (Harvey et al. 1986; Jones 1987). The mean free path of the highly relativistic degenerate electrons $d_{mfp} \sim c\tau_{sc}$, where $\tau_{sc} = \frac{H_{c2}}{B_c}\tau_n$ is the electron relaxation time in the case of proton superconductor core, $H_{c2} = \frac{\phi_0}{2\pi\xi^2} \sim 3 \text{ x } 10^{16}$ G is the upper critical field of the proton superconductor , $\tau_n \sim 2 \text{ x } 10^2 \ T^{-2}$ s is the electron relaxation time in the case of normal protons, T is the temperature of the

interior of the star. A typical value of T $\sim 10^8$ K gives $d_{\rm mfp} \sim 10$ cm. On the other hand, for scattering centers, namely fluxoids, each of a width $\lambda_{\rm p} \sim 10^{-11}$ cm having a mean separation of $d_{\rm f} \sim 10^{-10}$ cm the mean distance between successive encounters of electrons $d_{\rm enc} \sim d_{\rm f} \frac{d_{\rm f}}{\lambda_{\rm p}} \sim 10^{-8}$ cm. The polyhedra of the repeated deflections each of an angle $\sim \theta_0$ and of a polyhedral side $\sim d_{\rm enc}$ may be approximated by a circle of a radius $r_{\rm B}$ such that $d_{\rm enc} \sim \theta_0\, r_{\rm B}$. Thus $r_{\rm B} = \frac{d_{\rm f}^2 E_{\rm F}}{\lambda_{\rm p}^2\, e\, H_{\rm c1}}$, which upon substituting for $H_{\rm c1} \sim \frac{\phi_0}{\lambda_{\rm p}^2}$, and $d_{\rm f}^2 \sim \frac{\phi_0}{B_{\rm c}}$ may be reduced to $r_{\rm B} \sim \frac{E_{\rm F}}{e\, B_{\rm c}} \sim 3 \times 10^{-7}$ cm. *The latter expression shows that $r_{\rm B}$ is same as the radius of gyration of electrons in a uniform field same as the average field of the core of the star.* Hence, during *a* relaxation time, $\tau_{\rm sc}$, electrons make $\sim \frac{d_{\rm mfp}}{d_{\rm enc}} \sim 10^9$ encounters with fluxoids and complete $\sim \frac{d_{\rm mfp}}{2\pi r_{\rm B}} \sim 10^6$ gyration cycles round the fluxoids. *The lattice of fluxoids is therefore expected to be frozen in the electron gas* as would be the case for the uniformly distributed flux equivalent to that carried by all of the fluxoids in the MHD approximation of a highly conducting fluids (for a discussion see Jones 1987; Harrison 1991).

A treatment of the coherent electron scattering by the fluxoid lattice suggests that indeed the classical result of a "frozen-in" flux is applicable; the relative velocity of electrons and the fluxoids turns out to be almost zero. Nevertheless, the expulsion of the fluxoids out of the core would not be still prohibited as long as the electron-current loops across the core-crust boundary are not excluded. The expulsion time scale calculated for the case of coherent scattering as determined by the Hall drift of the flux in the base of the crust is not much different than that based on the single fluxoid approximation using F_v as given in Eq. 3.10 (Jones 1987, 1988, 1991). Uncertainties about the distribution of the magnetic flux and the correct value of the conductivity of the crust, and also the possibility of a mechanical failure of the solid crust due to a build-up of magnetic stresses however obscure any definite conclusion to be drawn. One may conclude that eventhough these studies suggest that whether or not flux can be expelled out of the core will be decided by the behavior of the currents at the core-crust boundary layer, the expulsion rate itself should be determined by the dynamics of the fluxoids and not from the boundary conditions alone. In our opinion, the importance

of collective effects is still controversial and the last word has not been said ! (see also Ding et al. 1993; Ruderman 1995).

Finally, we would like to draw attention to the following two points which have not been discussed in this context and which might be of some importance . The finite volume of the fluxoid lattice and the superconductor boundary effects on the motion of the fluxoids might allow for a different behavior than of those embedded within the electron gas. Secondly, the permitted motion of the lattice of fluxoids for the case with currents present at the core boundary (Jones 1991) would be nevertheless one with a nonzero divergence as the lattice constant is changing. In contrast the motion of the incompressible electron fluid in the interior of a neutron star is expected to be divergence free as pointed out by Goldreich & Reisenegger (1992). A relative motion between electrons and the fluxoids is therefore inescapable if any flux expulsion is to be assumed.

In the light of the above uncertainties, the value of F_v given in Eq. 3.10 will be therefore adopted for the drag force due to the electron scattering in our models. We note however that consideration of the coherent electron scattering has been shown to imply a maximum velocity for the flwoids outward motion (Jones 1991). On the other hand in some of our models which will be described later on (models B1 and B2 in Table 1 below) a similar value for a constraining maximum velocity of the fluxoids has been invoked, eventhough for a different reason. These models might be therefore expected to represent also the effects of considering a drag force due to the coherent electron scattering.

The buoyancy force:

The buoyancy force on fluxoids in a neutron star arises for reasons analogous to the case of macroscopic flux tubes in ordinary stars. Because flux tubes are in *pressure equilibrium* with the surrounding the excess magnetic pressure inside a flux tube causes a deficit in pressure and density of the plasma compared to the surrounding fluid. The tube will thus rise buoyantly due to the existing pressure gradient which supports the

hydrostatic equilibrium of the star against its gravitation. The force per unit length of a flux tube is given as

$$F_{\rm buoyancy} = A\ g\ \Delta\rho \tag{3.11}$$

where A is the tube cross section area, g is the local gravitational acceleration, and Ap is the difference in the density between the inside and outside of the tube (Parker 1979, chapter 8). For the fluxoids in the interior of a neutron star $A = \pi\lambda_{\rm p}^2$, Ap $= c_{\rm s}^{-2}\Delta P_{\rm s}$, the pressure difference $\mathbf{A}P_{\rm s} = \frac{H_{\rm c1}^2}{4\pi}$, and $\frac{c_{\rm s}^2}{g} \sim R_{\rm c}$, where $c_{\rm s}$ is the local sound speed. The buoyancy force per unit length of a fluxoid $F_{\rm b}$ which is directed radially outward can be expressed as (Muslimov & Tsygan 1985)

$$\begin{aligned} F_{\rm b} &= \left(\frac{\phi_0}{4\pi\lambda_{\rm p}}\right)^2 \frac{\ln(\lambda_{\rm p}/\xi)}{R_{\rm c}} \\ &= 0.51\ \text{dyn cm}^{-1} \end{aligned} \tag{3.12}$$

where values of $\lambda_{\rm p} = 131.5$ fm and $\frac{\lambda_{\rm p}}{\xi} = \sqrt{2}$ have been used. Note however that smaller values of $\frac{c_{\rm s}^2}{g} \sim 0.1R_{\rm c}$ have been also assumed in the literature (Muslimov & Tsygan 1985) which result in a larger value for $F_{\rm b}$.

Harrison (1991) has raised objection against the relevance of the buoyancy force for the fluxoids in the core of neutron stars. However, his argument is based on the premise of a frozen-in lattice of fluxoids in the electron-proton plasma within the star. In this case the buoyancy force is argued to contribute to the gradient of the macroscopic magnetic stresses supporting the hydrostatic equilibrium of the plasma within the star. His argument does not of course apply to the case where relative motion of the fluxoids and the plasma is allowed to take place, as we have assumed. We will therefore take into account the buoyancy force on the fluxoids in our model calculations. Ding et al. (1993) whose study also assumes independent motions of single fluxoids have argued that fluxoid motion might be so fast that hydrostatic-equilibrium conditions and hence Harrison's objection against the buoyancy force in neutron stars might be avoided. We don't find this argument self-consistent. Either one assumes the fluxoid lattice to be frozen into the plasma in which case the buoyancy force contributes to the hydrostatic pressure and results in inflation of the plasma as pointed out by Harrison (1991), or

if the relative motion of the fluxoid with respect to the electron gas is assumed there exists no question about the effectiveness of the buoyancy force (see in particular last paragraph before § 3.2, p. 422 in Harrison 1991). Furthermore, it is hard to see why the hydrostatic equilibrium in the core of a neutron star would be approached, as speculated by Ding et al. (1993), at a speed less than 10^{-7} cm s^{-1} which is the largest typical speed predicted for the fluxoids. This would imply an absurdly large time scale for the hydrostatic equilibrium of a neutron star $\gtrsim 1$ Myr in contrast to its dynamical time scale $\sim \left(\frac{1}{G\rho}\right)^{\frac{1}{2}} \sim 10^{-3}$ s. Notice that the sound speed in the interior of a neutron star is calculated to be $\sim 10^{8}$ cm s^{-1} for the case of a normal non-superfluid core and $\gtrsim 10^{9}$ cm s^{-1} if a superfluid component is present (Epstein 1988).

The curvature force :

The kinetic energy per unit length of a superfluid vortex is $T \sim \left(\frac{\rho\kappa^2}{4\pi}\right) \ln \frac{D}{\xi}$ where D is a macroscopic cutoff distance that represents either the size of the container or the distance between vortices (Fetter 1976). Although the tension of the vortex line is not always exactly equal to its energy per unit length, in the limit of long wavelength disturbances the equality does hold (Fetter 1976, Baym & Chandler 1983). For proton superconductor fluxoids the currents are screened away within a distance $\sim \lambda_p$ which is the corresponding cutoff length ($D = A$). Substituting for the vorticity $\kappa \equiv \frac{e\,\phi_0}{c\,m_p}$, and $\lambda_p = \left(\frac{m_p^2\,c^2}{4\pi\,e^2\,\rho}\right)^{\frac{1}{2}}$ one gets $T_p \sim \left(\frac{\phi_0}{4\pi\lambda_p}\right)^2 \ln \frac{\lambda_p}{\xi}$ for the tension of the fluxoids (Nozieres & Vinen 1966; Harvey et al. 1986; see however De Gennes 1966 for a different derivation based on integration of the electromagnetic energy density of a flwoid in a type-I1 superconductor).

As in a mechanical system the tension of a vortex line implies that a curved geometry of the line would result in a restoring force, called "curvature" force, which tries to bring the line back to the minimum energy straight configuration. The concavely directed "curvature" force per unit length of a vortex F_c having a tension T and a radius of curvature S_c is given as $F_c = \frac{T_p}{S_c}$ (Harvey et al. 1986). This is similar to the curvature force on magnetic field lines embedded in a conducting fluid which is

defined in a similar way (Parker 1979, chapter 5). The curvature force on a vortex line may be also derived on an apparently different basis. A curved vortex is subject to an additional induced motion perpendicular to the plane of the vortex which will result in a corresponding Magnus force that has the same magnitude and the same direction as the above curvature force (Batchelor 1967, p. 510).

For a fluxoid in a neutron star with tension T_p the curvature force can be expressed in terms of the buoyancy force F_b (see **Eq.** 3.12) as follows :

$$\begin{aligned} |F_c| &= \frac{R_c}{S_c}\left(\frac{\phi_0}{4\pi\lambda_p}\right)^2 \frac{\ln(\lambda_p/\xi)}{R_c} \\ &\equiv \frac{R_c}{S_c} F_b \end{aligned} \tag{3.13}$$

where R_c is the radius of the core of the star. The end points of a fluxoid, where its magnetic flux spouts out and joins the almost uniform field of the crust are expected to be "frozen-in" at the bottom of the crust due to the large conductivity of the matter. An outward moving fluxoid is therefore expected to be bent outward and subject to a force F_c which is directed inward, namely $F_c = -\frac{R_c}{S_c} F_b$. For a spatially uniform distribution of the fluxoids the estimated average value of $\frac{R_c}{S_c} \sim \ln 2$ (Ding et al. 1993). Substituting in **Eq.** 3.13 and using **Eq.** 3.12 the inward curvature force per unit length of a fluxoid is found to be

$$F_c = -0.35 \ \text{dyn cm}^{-1} \tag{3.14}$$

In contrast, Muslimov & Tsygan (1985) suggested a value of $F_c \sim -0.1 F_b$ due to the larger value they adopted for F_b compared to that given by **Eq.** 3.12, and Harvey et al. (1986) used $F_c \sim -F_b$ for the outer parts of the core. Ding et al. (1993) assumed that the fluxoids would be bent outward during times $t < \tau_{Ohm}$ and, conversely, (in effect) bent inward at all later times $t > \tau_{Ohm}$, where τ_{Ohm} is the assumed time scale for the decay of the magnetic field in the crust. An inward force F_c as in Eq. 3.14 is hence adopted in their model only during times $t < \tau_{Ohm}$, while for $t > \tau_{Ohm}$ an outward force of a comparable magnitude has been assumed to be effective.

The latter (outward) force which implies an spontaneous motion of the end points of a fluxoid at a speed faster than the fluxoid itself will be however ignored in the

alternative models which we have considered. The assumed tendency of a flux tube for decreasing its length under the effect of its tension (Harvey et al. 1986) does not seem to satisfy by itself the requirements for realizing such a geometry of inward bending lines continuously at all times $t > \tau_{\rm Ohm}$. Or equivalently, considering the negligible radius of a fluxoid as compared to the radius of the curvature of its boundary surface the gain in energy due to outward motion does not imply an *instantaneous* force to be effective.

Furthermore, in our models the time constraint used by Ding et al. (1993) for the outward bending of the fluxoids namely, $t < \tau_{\rm Ohm}$ is replaced by a condition on the velocity of the lines as compared to a maximum speed $v_{\rm max}$ permitted for the motion of their end points by the conductivity of the matter in the crust. It will be assumed that whenever the condition $v_{\rm p} < v_{\rm max}$ is satisfied the end points of the fluxoids in the crust are able to follow the motion of the fluxoids, thence they remain straight and *no* "curvature" force will be acting on them. In the opposite case when $v_{\rm p} \geq v_{\rm max}$ the fluxoids are however expected to be bent outward and the force $F_{\rm c}$ as in Eq. 3.14 would be effective. We note that a self-consistent solution of the equation of motion given below (Eq. 3.18) is however found to require that the transition between the above two realizations of $F_{\rm c}$ for $v_{\rm p} \geq v_{\rm max}$ and $v_{\rm p} < v_{\rm max}$ occurs gradually (see Fig. **3.4** below), which is also a more physically plausible behavior than a discontinuous jump at $v_{\rm p} = v_{\rm max}$. The maximum drift velocity of the magnetic flux in the crust $v_{\rm max}$ is estimated as

$$v_{\rm max} \sim \frac{R}{\tau_{\rm Ohm}} = 3.18 \times 10^{-9} \left(\frac{\tau_{\rm Ohm}}{10^7 {\rm yr}} \right)^{-1} \ {\rm cm\ s^{-1}} \qquad (3.15)$$

where R is the radius of a neutron star and $R = 10^6$ cm has been used, and $\tau_{\rm Ohm}$ is in units of yr. **A** larger value for $v_{\rm max}$ may be however expected if the effects due to the Hall drift of the magnetic field at the bottom of the crust is taken into account. The suggested mechanical failure and plate tectonic motion of the crust itself (Ruderman 1991) if it is driven by some other effectrather than the pull of the fluxoids on the crust,

implies a separate model in which only $v_p \geq v_{plate}$ is allowed, where v_{plate} is the assumed velocity of crustal plates motion. However, in the cases where the motion is argued to be driven by the motion of fluxoids themselves (Ruderman 1991) no additional restrictions is required in our models.

On the other hand, it has been argued that the repulsive force between the fluxoids should ensure that the lattice response to a deformation is determined, to a first approximation, by their collective rigidity (Jones 1991). The force F_c associated with even a piece of the lattice which lies between successive neutron vortices (typically extending over some 10^7 flux lines) would be, in this approximation, so large that any bending of the lattice is effectively prohibited. The velocity of the fluxoids would be therefore constrained at all times by the condition $v_p \leq v_{max}$, with $F_c = 0$. In this approximation, if the conditions are such that a value of $v_p > v_{max}$ is implied for $F_c = 0$ then $v_p = v_{max}$ will be assumed, and F_c is calculated from

$$F_c = -[F_n + F_b + F_v] \tag{3.16}$$

where the right hand side is evaluated for $v_p = v_{max}$, and $w = \omega_{cr}$ or $= -\omega_{cr}$, whichever is the case. The above prescription for calculating F_c might be alternatively justified as being due to the extremely large viscous drag force in the case of coherent scattering discussed earlier.

We will consider different models for determining the fluxoids velocity in which either of the two estimates for F_c (Eqs 3.14 or 3.16) are adopted, alternatively (see Table 1 below).

Magnetic scattering of electrons off fluxoids results also in a component of the drag force perpendicular to the direction of the relative motion (Harvey et al. 1986) which is interpreted also as a Lorentz retarding force acting on fluxoids (Harrison 1991; Jones 1991). For a radial motion of fluxoids this component of the drag force is expected to be canceled by the azimuthal Magnus force on fluxoids due to their motion with respect to the proton superconductor (Jones 1991). These two forces as well as a radial force due to electron-proton Coulomb scattering which is much smaller than the other forces of interest (Jones 1987) are hence neglected.

3.2.4 The Models

The steady-state radial motion of a fluxoid in the region of interest (cf. § **3.2.2)** is thcs determined from the balance equation for all the radial forces, per unit length, acting on it

$$F_{\rm n} + F_{\rm v} + F_{\rm b} + F_{\rm c} \;=\; 0 \qquad (3.17)$$

Substituting for the different terms from Eqs 3.5 or 3.7, 3.10, 3.12, and 3.14 or 3.16, respectively, the above equation may be rewritten in the form

$$\alpha\,\frac{\omega_{-6}}{P_{\rm s}B_3} - \beta\,v_{\rm p_7} + \delta = 0 \qquad (3.18)$$

where parameters α, β, and $\delta(\equiv F_{\rm b} + F_{\rm c})$ are given below for the different models, and $v_{\rm p_7}$ is the fluxoid velocity $v_{\rm p}$ in units of 10^{-7} cm s^{-1}. Recall that ω_{-6} which is the value of $\omega(\equiv \Omega_{\rm s} - \Omega_{\rm L})$ in units of 10^{-6} rad s^{-1} might have either positive or negative values, as is the case for δ in some of the models.

This equation includes two unknown variables w and $v_{\rm p}$ and represents the *azimuthal component of the Magnus equation* of motion for the proton vortices. The right hand side is zero because there is no radial Magnus force being exerted by the superconductor on the fluxoids, due to the assumed co-rotation of the fluxoids with the proton superconductor. There exist however additional restrictions on the motion of the fluxoids which can be used to fix the value of one of the variables in Eq. 3.18 and solve for the other. Namely, in a co-moving state $v_{\rm p} = v_{\rm n}$ thus Eq. 3.18 can be be solved for w. And, in the other two alternative cases where $v_{\rm p}$ is unknown w could take only either of the two values $w = \omega_{\rm cr}$ or $w = -\omega_{\rm cr}$ depending on $v_{\rm p} < v_{\rm n}$ or $v_{\rm p} > v_{\rm n}$, respectively. Furthermore, inspection of the Eq. 3.18 indicates that only one of the above three solutions (viz., $v_{\rm p} = v_{\rm n}$, $w = \omega_{\rm cr}$, or $w = -\omega_{\rm cr}$) can be satisfied at any time, for given values of the variables $v_{\rm n}, B_{\rm c}$, and $P_{\rm s}$. The rate of the flux expulsion out of the core $\dot{B}_{\rm c} = -\frac{2}{R_{\rm c}}B_{\rm c}v_{\rm p}$, and the evolution of the stellar field $\dot{B}_{\rm s}$ (with a decay rate of $\dot{B}_{\rm s} = -\frac{B_{\rm s}-B_{\rm c}}{\tau_{\rm Ohm}}$) are hence uniquely determined from the above force balance equation (Eq. 3.13), for an assumed spin evolution of the star which determines the vortex velocity $v_{\rm n}$ at *each* time (Eq. 3.2).

Based on the two alternative estimates discussed in the previous subsections for each of the pinning F_n and curvature F_c forces acting on the fluxoids in the interior of a neutron star, we have considered four separate models by permutation, which are labeled A1, A2, B1, and B2. The underlying assumptions which lead to these alternative evaluations of the forces, discussed earlier, are

- pinned *segments* of a vortex may creep independently $\leftrightarrow$ vortex remains *straight* while creeping
- fluxoids may bent if moving *faster* than a given maximum velocity $\leftrightarrow$ (fluxoids are never bent $\equiv$) fluxoids velocity *cannot exceed* the given maximum value

The models are summarized below by indicating which of the above four assumptions are adopted in each case. Also the values of the parameters in the single force equation (Eq. 3.18), which is the starting point for computing the field evolution in all the models, are given for each of them.

- Model A1: $\begin{cases} \text{- vortex } \textit{segments} \text{ creep independently} \\ \text{- fluxoids are } \textit{bent} \text{ when } v_{\rm p} > v_{\rm max} \end{cases}$

  $\alpha = 5.03,$

  $\delta = \begin{cases} 0.51 & \text{if } v_{\rm p} < v_{\rm max} \\ 0.16 & \text{if } v_{\rm p} \geq v_{\rm max} \end{cases}$

- Model A2: $\begin{cases} \text{- vortices remain } \textit{straight} \text{ while creeping} \\ \text{- fluxoids are } \textit{bent} \text{ when } v_{\rm p} > v_{\rm max} \end{cases}$

  $\alpha = 2.587 \times 10^{-4}\ B_8^{1/2},$

  δ = same as for A1

- Model B1: $\begin{cases} \text{- vortex } \textit{segments} \text{ creep independently} \\ \text{- fluxoids velocity } v_{\rm p} \leq v_{\rm max} \text{ always} \end{cases}$

  α = same as for A1,

  $\delta = \begin{cases} 0.51 & \text{if } v_{\rm p} < v_{\rm max} \\ -(F_{\rm n} + F_v) & \text{if } v_{\rm p} = v_{\rm max} \end{cases}$

  $v_{\rm p} > v_{\rm max}$ not permitted

- Model B2: $\begin{cases} \text{- vortices remain } \textit{straight} \text{ while creeping} \\ \text{- fluxoids velocity } v_{\rm p} \leq v_{\rm max} \text{ always} \end{cases}$

  α = same as for A2,

  δ = same as for B1

while $\beta = 7.30$ is the same for all the models

These four models together with the model adopted by Ding et al. (1993, the **DCC** model) will be referred to collectively as the FBE models (namely those which employ a Force Balance Equation), in contrast to the SIF model which follows a different treatment of the flux expulsion rate (see Table 1). Spin and magnetic evolution of single as well as binary pulsars are calculated according to the requirements of each of the models, separately, and the results are discussed in the following sections.

Table 3.1- Different models for the dynamics of the fluxoid motion

model		F_n	F_v and F_b	F_c	v_p and ω
FBE	DCC	as in Eq. 3.5	as in Eqs. 3.10 and 3.12	as in Eq.3.4 if $t < \tau_{Ohm}$ $= \frac{\pi}{4} F_b$ if $t \geq \tau_{Ohm}$	from Eq. 3.18, subject to :
	A1			$= 0$ if $v_p < v_{max}$ as in Eq. 3.14 if $v_p \geq v_{max}$	
	B1			$= 0$ if $v_p < v_{max}$ as in Eq. 3.16 if $v_p = v_{max}$	$v_p = v_n$ iff $\lvert\omega\rvert < \omega_r$
	B2	as in Eq. 3.5 if $v_p = v_n$		($v_p > v_c$ not permitted)	$\omega = \omega_r$ iff $v_p < v_n$
	A2	as in Eq. 3.7 if $v_p \neq v_n$		$= 0$ if $v_p < v_{max}$ in Eq. 3.14 if $v_p \geq v_{max}$	$\omega = -\omega_r$ iff $v_p > v_n$
SIF		$v_p = v_n$ (summed)			

3.3 Field Evolution of Single **Pulsars**

We shall now present the results of our model computations for the spin-magnetic evolution of single pulsars based on the models discussed in the previous section. The spin evolution of a solitary pulsar is assumed to be driven by a torque due to its magnetic dipole radiation and/or outflow of the relativistic charged particles which results in $\dot{P}_s = 3.15 \times 10^{-16}\ B_8{}^2/P_s\ \mathrm{syr}^{-1}$ (cf. Eq. 1.26), where B_8 is the surface field B_s in units of 10^8 G, and P_s is in units of seconds. The coupled evolution of the spin period and magnetic field are thus followed over a period of 10^{10} yr in order to cover both young and very old neutron stars in the Galaxy. The rate of the decay of the core field will be calculated from the value of the fluxoid velocity as determined in each of the FBE models discussed in the previous section. From the instantaneous value of the spin-down rate one finds the velocity v_n of the outward motion of the vortex (Eq. 3.2). Also, w, – the maximum absolute value of the lag w that might be supported by the pinning force – may be determined for any given value of the core field strength B_c from Eq. 3.8. The solution of Eq. 3.18 for the given values of v_n and ω_{cr} at a given time t then determines the corresponding values of the fluxoids velocity v_p and the lag w between the rotation rates of the vortices and the neutron superfluid in the core of the evolving solitary pulsar. As indicated in the previous subsection, Eq. 3.18 admits *one and only one* of the following three different solutions:

$$
\begin{array}{lcll}
w & = & \omega(v_p = v_n) & \text{iff} \quad -\omega_{cr} < w < \omega_{cr} \\
v_p & = & v_p(\omega = \omega_{cr}) & \text{iff} \quad v_p > v_n \\
v_p & = & v_p(\omega = -\omega_{cr}) & \text{iff} \quad v_p < v_n
\end{array}
$$

where in each case one of the two unknowns in Eq. 3.18 is given and the other one may be determined. Time evolution of v_p may thus be calculated by testing the above three solutions, in any order, and finding the appropriate one at each time. The computed time behavior for v_p and w are shown in Fig. 3.1 as predicted in the A1 model. Characteristically similar results as in Fig. 3.1 are obtained for the other FBE

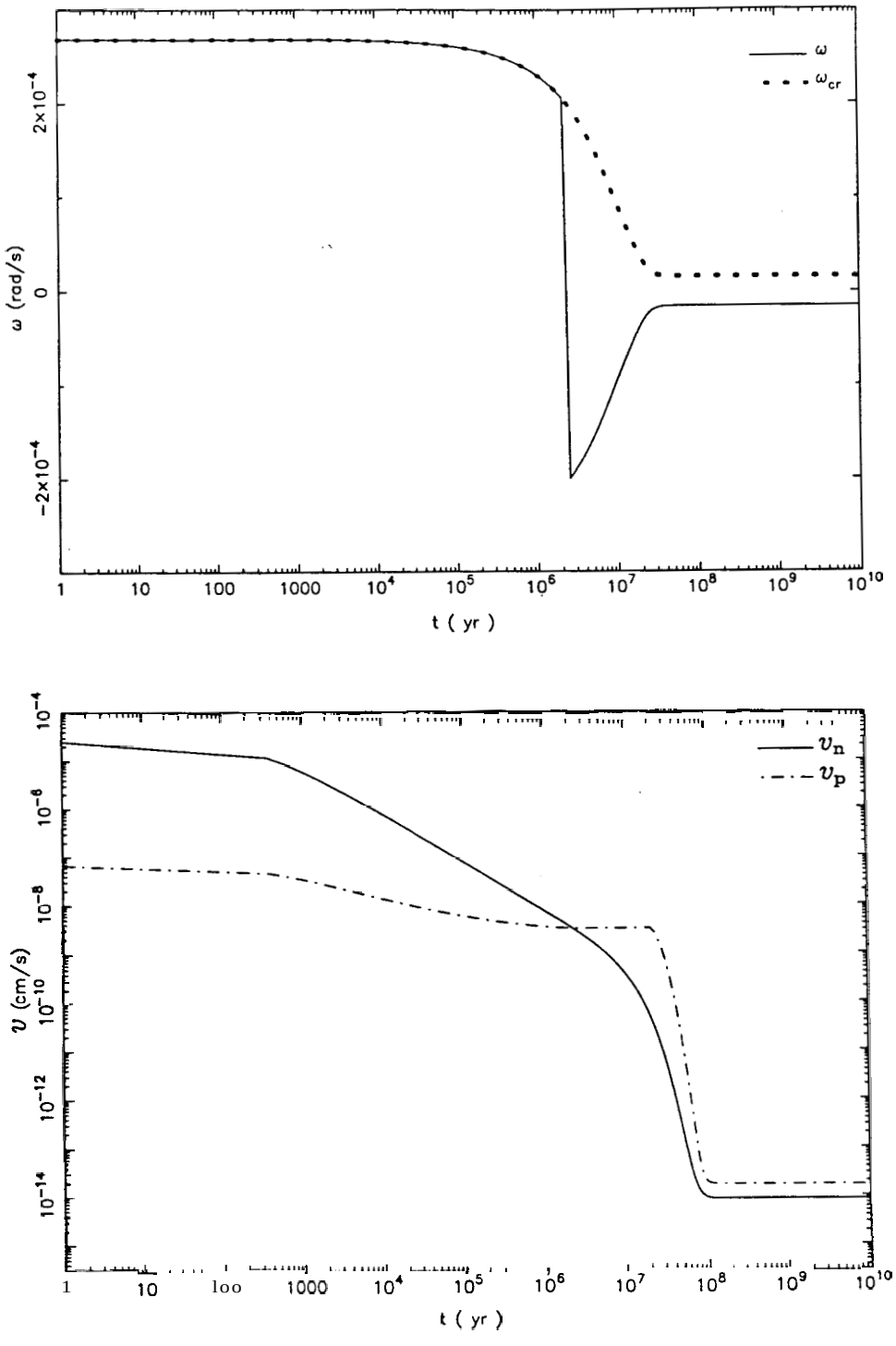

Figure **3.1**- The *top* panel shows the predicted time evolution of the lag w and its critical value ω_{cr} in a solitary neutron star according to the A1 model. The *bottom* panel shows the corresponding evolution of the velocity of the fluxoids v_p and vortices v,. Initial values of $B_s = 10^{12.5}$ **G**, $B_c = 0.9B_s$, and a value of $\tau_{Ohm} = 10^7$ yr have been used.

models described previously (§ **3.2.3).** We have also included in Fig. **3.1** the curves representing evolution of the velocity of neutron vortices v_n and the critical lag ω_{cr} in the appropriate panels, as indicated.

The fluxoids motion in Fig. **3.1** is seen to follow three evolutionary phases in which they move slower, together, and faster than the vortices, successively. These will be referred to as *forward* creep, co-moving, and reverse creep phases, respectively (we use the terminology of Ding et al. **1993).** A final co-moving phase might also occur for some choices of the initial conditions. Note that ω is negative during the reverse creep phase and the later parts of the co-moving phase. A change from positive to negative values for these quantities occurs during the co-moving phase. Also note that $|\omega| = \omega_{cr}$ during both the forward and reverse creeping phases. Transitions between these successive evolutionary phases occur due to a reduction in v_n $(\propto \Omega_s)$ as well as the increasing value of P_s.

Field behavior:

The rate of expulsion of the core field at any time is governed by v_p and therefore evolution of the core and the surface field strengths may be determined corresponding to the history of the fluxoid velocity given in Fig. 3.1. The predicted field evolution of a single neutron star according to the A1 model (which is similar to that due to other FBE models) may be seen in Fig. **3.2.** Evolution of the spin period is also plotted in Fig. **3.2,** and Fig. 3.2a corresponds to the results in Fig. **3.1.**

A substantial decrease in the core magnetic field strength occurs at times $t \gtrsim 10^7$ yr, due to the typical average value of $v_p \lesssim 10^{-8}$ cm s^{-1} during this period (see Eq. **3.18).** Recall that $\frac{B_s}{B_c} = \frac{v_p}{R_c}$ which implies a time period of **At** $\sim \frac{R_c}{v_p}$ for a major reduction in the core field to occur. As a result of the very small magnitude of v_p (although $\gtrsim v_n$) and the reduced value of B_c at all later times, there is no substantial change in B_c subsequently.

The surface field B_s responds to the change in B_c on the assumed decay time scale τ_{Ohm} of the crust. A value of 10^7 yr has been assumed for τ_{Ohm} in Fig. 3.2a. The effect

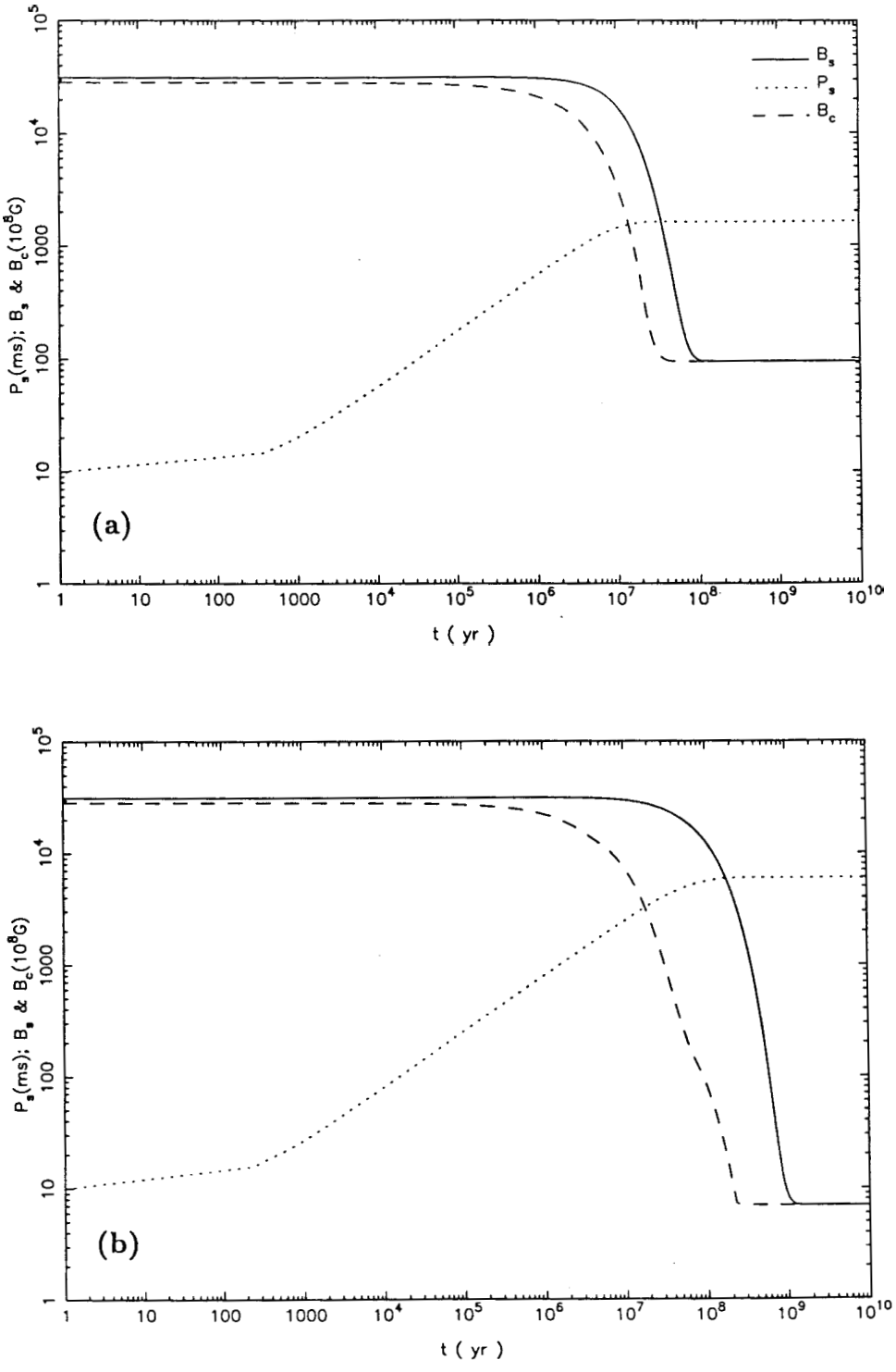

Figure **3.2**- The predicted time evolution of the strength of the magnetic field in the core B_c and at the surface B_s, and the spin period P_s in a solitary neutron star according to the A1 model. **(a)** is for an assumed value of $\tau_{\rm Ohm} = 10^7$ yr and corresponds to the results in Fig. 3.1, and **(b)** is for $\tau_{\rm Ohm} = 10^8$ yr.

of the value of τ_{Ohm} on the predicted field evolution of neutron stars may be seen by comparing Fig. 3.2a with Fig. 3.2b where for the latter we have assumed a value of $\tau_{Ohm} = 10^8$ yr. A larger value of τ_{Ohm} results in large B_s over an extended period of time which corresponds to larger $|\dot{\Omega}|$ and hence larger v_n. Consequently the predicted evolution of the spin period of the star leads to larger values of the rotation period for a larger choice of τ_{Ohm}. This results in a smaller final value for B_c (note the inverse dependence on $P_s B_c$ in Eq. 3.18 which is further discussed below).

Fig. 3.2a seems to suggest that B_s stops decaying when B_c starts to decline (indeed, this has been asserted by Ding et al. 1993). However this is an artifact of the assumed value of τ_{Ohm} which happen to be close to the saturation time of the core field decay. The spurious correlation between the time when the core field stops decaying and the value of τ_{Ohm} may be confirmed by using tentatively smaller values of $\tau_{Ohm} \lesssim 10^6$ yr in which case the core and surface fields are seen to decay simultaneously as seen in Fig. 3.3. Rather, the core field stops decaying as a result of decreasing values of v_p as well as B_c itself.

3.3.1 Flux expulsion: which is the "Driving" Force?

It is interesting to note that the major flux expulsion occurs (compare Fig. 3.1 with Fig. 3.2a) during the co-moving and, particularly, the reverse creep phases. This means that the dominant "driving" force for the flux expulsion is the buoyancy force (together with the tension force in the case of the DCC model). In Fig. 3.4 the time evolution of the forces acting on the fluxoids is shown for the different models, separately. In each plot the three curves correspond to the time behavior of the pinning, drag, and buoyancy plus curvature forces acting on unit length of fluxoids close to the core-crust boundary. The four plots in Fig. 3.4 show the results for the models A1 (which corresponds to the results in Fig. 3.1 and Fig. 3.2a), A2, B1, and DCC, separately, while those of B2 are similar to A2 and are excluded.

The pinning force F_n is seen to be negative and directed inward during the reverse creep phase and the later part of the co-moving phase. Hence, the overall effect of the

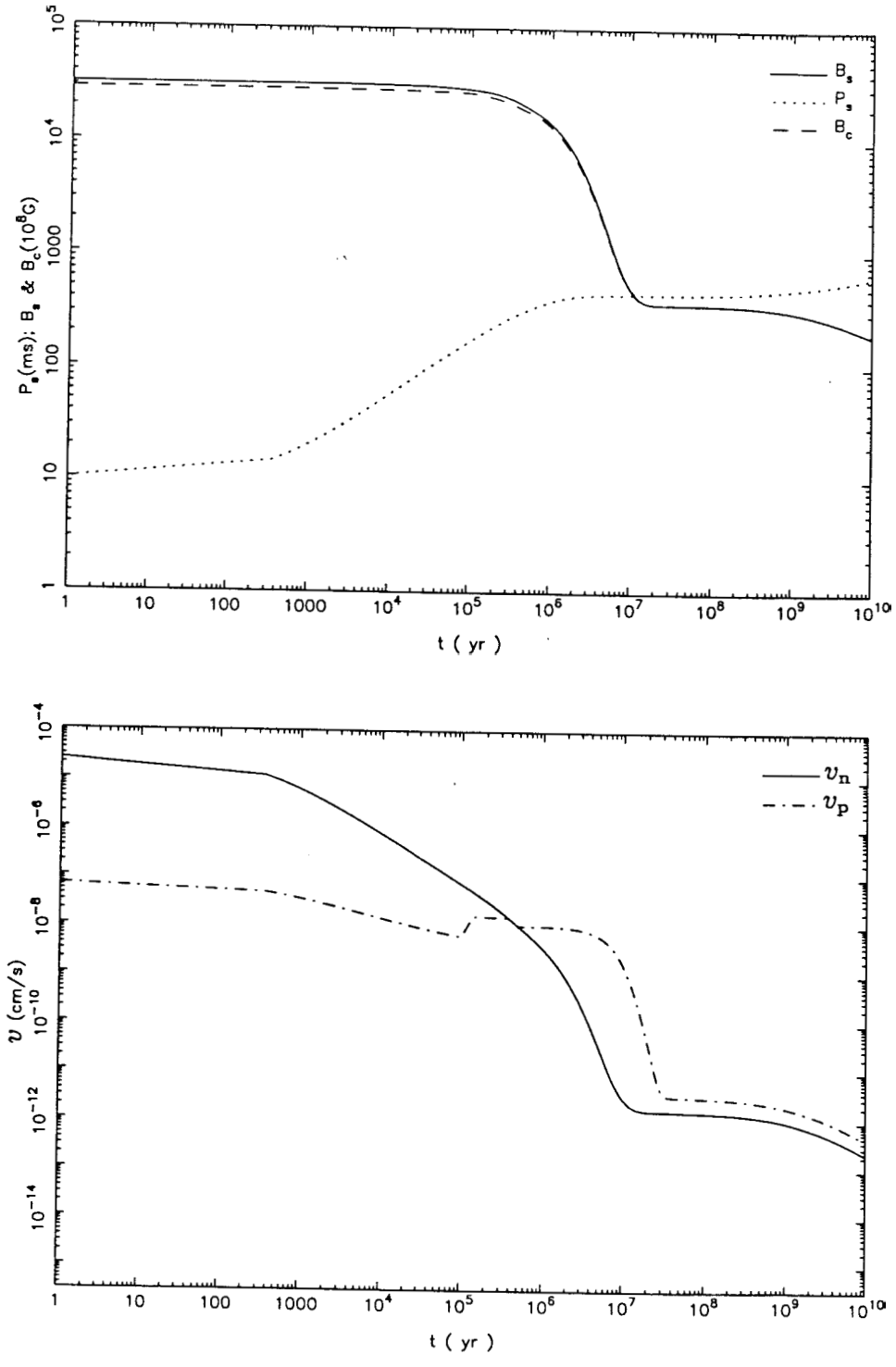

Figure **3.3-** The evolution of the spin period and the strengths of core and surface magnetic fields *(top)*, and that of the velocities of the fluxoids and vortices *(bottom)* as in Fig. 3.2a and Fig. 3.1, respectively, but for an assumed value of $\tau_{\rm Ohm} = 10^5$ yr. The DCC model has been used for the purpose of the discussion but the behavior is the same for the other FBE models as well.

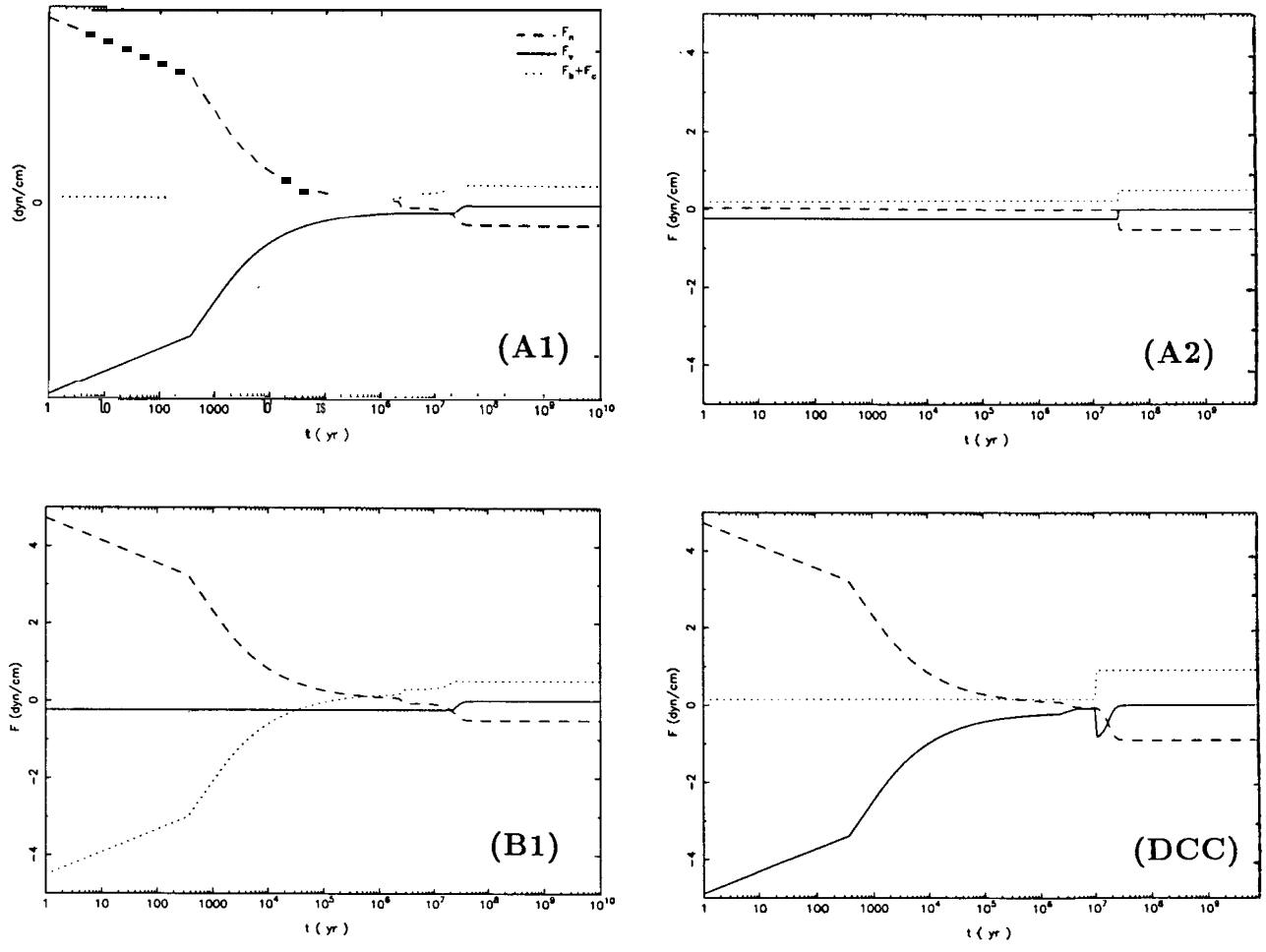

Figure 3.4- The predicted time evolution of the various forces acting radially on fluxoids (per unit length) in a solitary neutron star, according to the different FBE models. The pinning force $F_{\rm n}$, the drag force F_v, and sum of the buoyancy plus curvature forces $F_{\rm b}+F_{\rm c}$ are shown in each panel. The force evolution shown for the A1 model corresponds to the results in Fig. 3.1 and Fig. 3.2a, and the same values of the parameters have been used for all the models.

pinning force for the field decay of solitary pulsars is more like a "brake" *preventing the flux to be to expelled too rapidly*. This conclusion is in contrast to what might have been expected at the outset for the role of the pinning force as a driving cause of the flux expulsion. Indeed, Ding et al. (1993) attribute such a driving role to the pinning force throughout their paper, which is not correct as is further discussed in the following.

Although the above conclusion about the role of the pinning force seems to be obvious from the results in Fig. 3.4 (and also from velocity and field plots in Fig. 3.1 and Fig. 3.2), it may be further demonstrated by other tests of model calculations. We will present the results of these tests in Figs 3.5a, 3.5b, and 3.5d within the **DCC** model, however other FBE models produce similar results. *Fig. 3.5a which is for the case of setting* $F_n = 0$ *in the model calculations shows that in the absence of the pinning force almost all of the core flux is expelled within a time scale of* $\sim 10^7$ *yr.* In contrast, Fig. 3.5b shows that for an assumed case of $F_b + F_c = 0$, in which case the force F_n is directed outward all the time, the field decays by only less than an order of magnitude within 10^{10} yr. Since the buoyancy and curvature forces are not invoked in the SIF model it is appropriate to compare Fig. 3.5b with predictions of the SIF model for the same assumed parameter values. Fig. 3.5c shows that field decay is more in SIF than for the case with $F_b + F_c = 0$ in FBE models (Fig. 3.5b). The difference is due to the smaller values of v_p at early times in Fig. 3.5b than that implied by in Fig. 3.5c which is due to the presence of the drag force in the present calculation. Yet another demonstration of the retarding effect of the pinning of fluxoids and vortices on the expulsion of the magnetic **flux** might be seen from a comparison between the results for different assumed values of the pinning energy E_P. In Fig. 3.5d the results due to two cases with assumed values for E_P being 10 times smaller and 10 times larger than that used in all other Figures (in particular Fig. 3.2a) are shown. Note that in addition to the plot for the field and period evolution we have also included in Fig. 3.5d the plot for the force evolution in one case and for the velocity in another case. Comparing the two cases in Fig. 3.5d, and also with Fig. 3.2a which is for the value of E_P intermediate

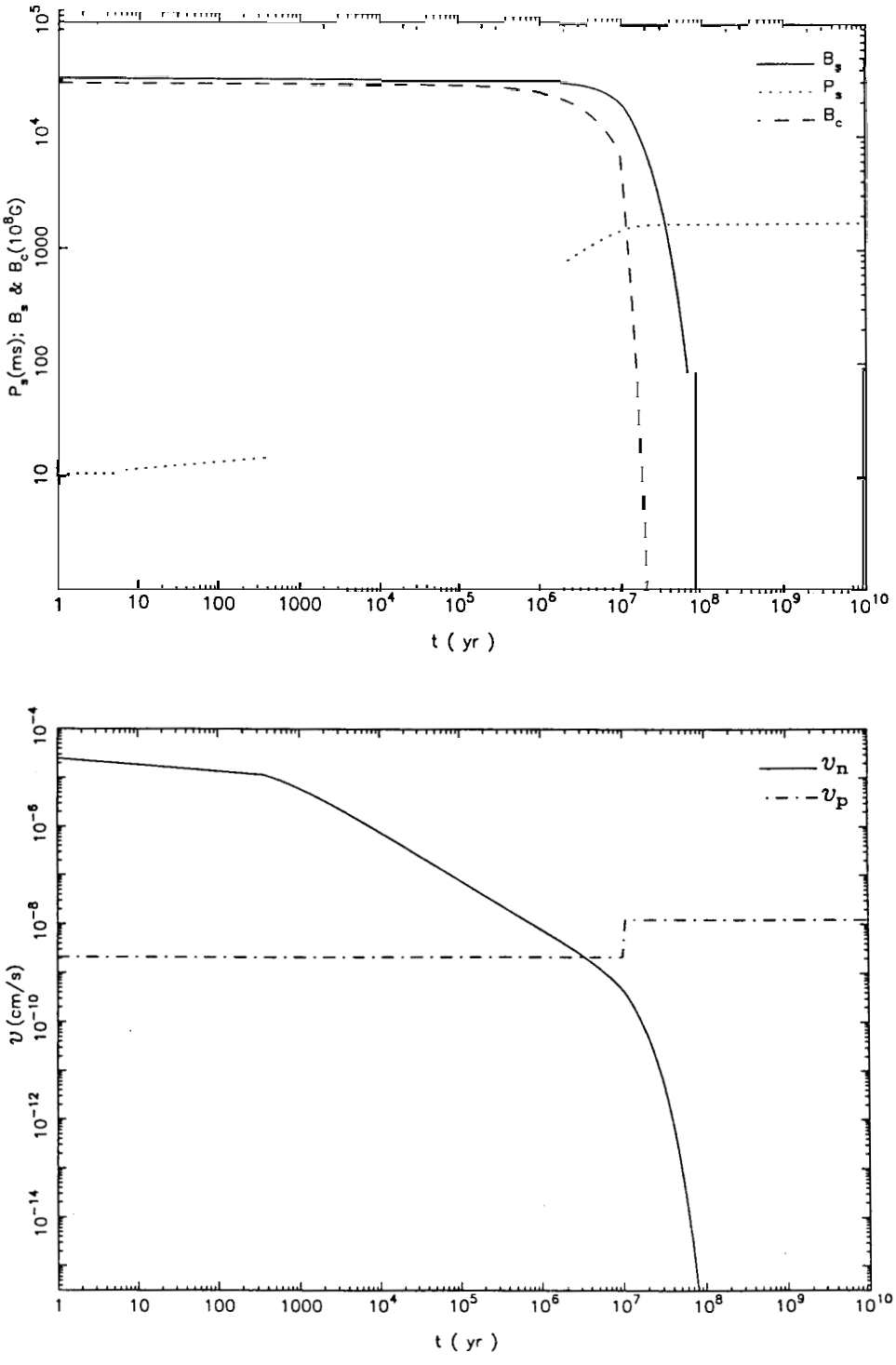

Figure 3.5(a)- The spin-magnetic field, and the velocity plots as in Fig. 3.2a and Fig. 3.1 and for the same values of the parameters (particularly $\tau_{\rm Ohm} = 10^7$ yr) but for an assumed case of $F_{\rm n} = 0$ throughout the evolution of the star. The DCC model has been used for the purpose of the discussion but the behavior is the same for the other FBE models as well.

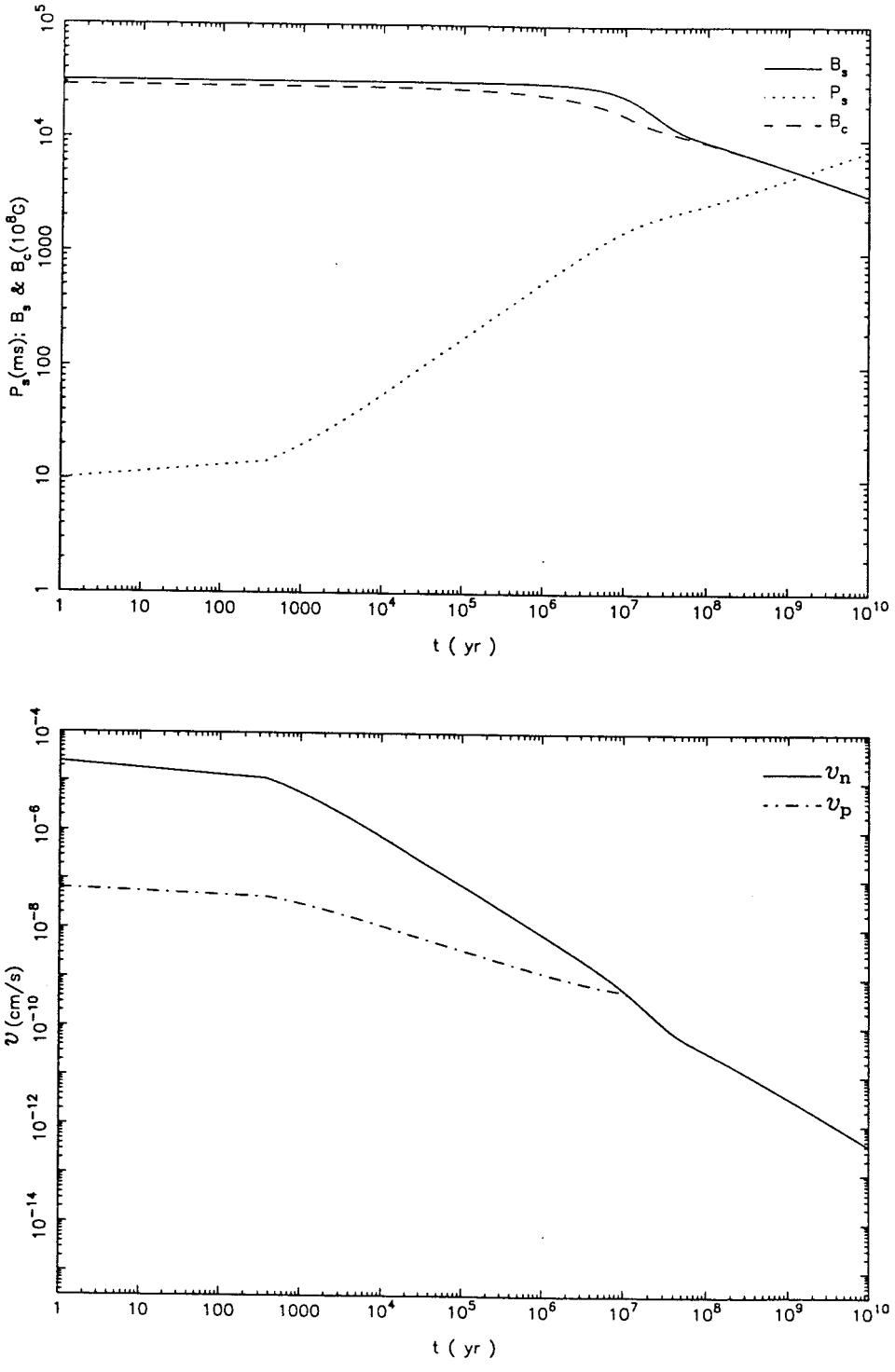

Figure 3.5(b)- The spin-magnetic field, and the velocity plots as in Fig. 3.2a and Fig. 3.1 but for an assumed case of $F_b + F_c = 0$ throughout the evolution of the star. The DCC model has been used for the purpose of the discussion but the behavior is the same for the other FBE models as well.

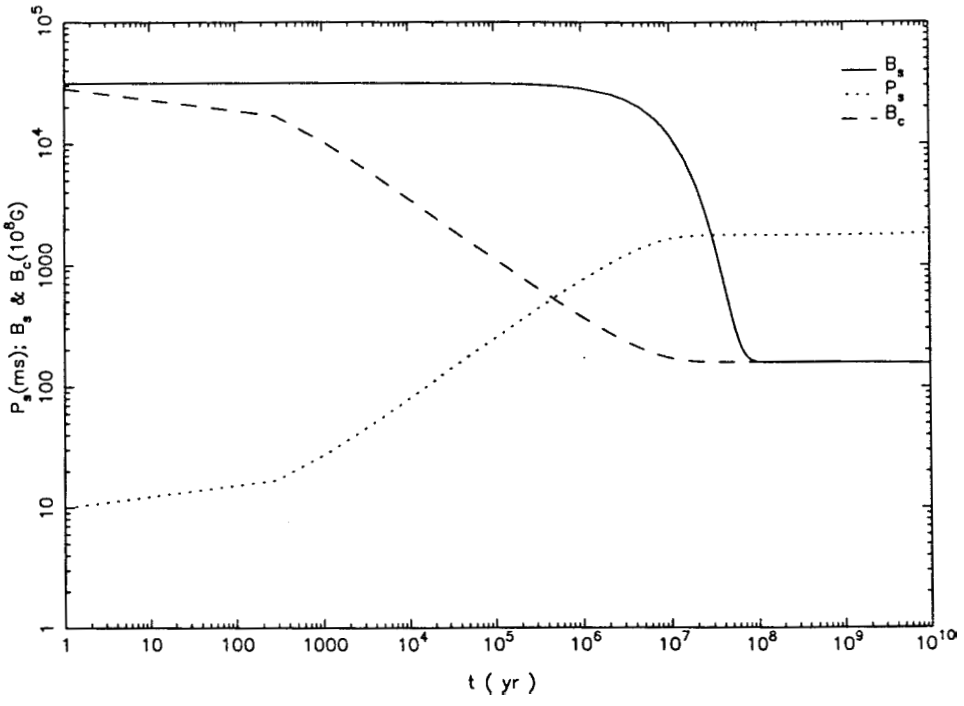

Figure 3.5(c)- The spin-magnetic field evolution as predicted in the SIF model. Same parameter values as in Fig. 3.5b have been used.

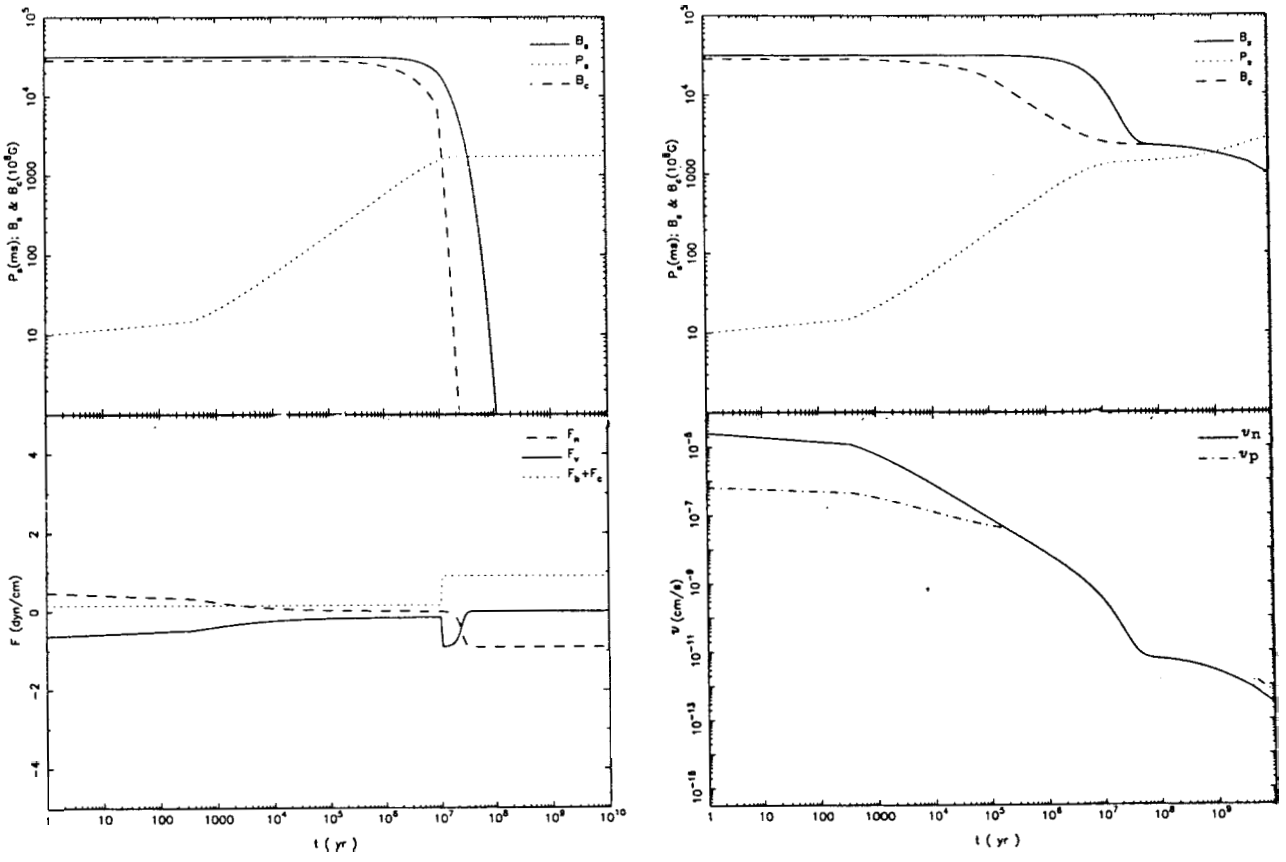

Figure **3.5(d)-** The *left* two panels show the spin-magnetic field, and the force plots as in Fig. 3.2a and Fig. 3.4 but for an assumed 10 times smaller value of the pinning energy $E_{\rm P}$. The *right* panels show the spin-magnetic field, and the velocity plots as in Fig. 3.2a and Fig. 3.1 but with an assumed 10 times larger value for the pinning energy $E_{\rm P}$. The DCC model has been used for the purpose of the discussion but the behavior is the same for the other FBE models as well.

to those in Fig. 3.5d, shows that the amount of the expulsion is less for an assumed larger value of E_P that supports a stronger pinning force (compare the force behavior with that in Fig. **3.4).** This again indicates that the opposing role played by the pinning force against the outward motion of the fluxoids is dominant over its contribution, at the earlier times of a pulsar lifetime, to the "driving" causes of flux expulsion.

Therefore, the fact that the final value of B_c is smaller for larger values of τ_{Ohm} may not be explained in terms of F_n acting more efficiently to expel the flux, which is the explanation given by Ding et al. (1993). Instead, it is because larger values of τ_{Ohm} have the effect of resulting in larger values of P_s and hence smaller residual field strengths. Consulting Eq. 3.18 one might verify that the combination $P_s B_c$ (or $P_s B_c^{\frac{1}{2}}$ in **A2** *and* B2 models) is the deciding factor in determining the value of v_r. Ding et al. (1993) further state that in comparison to the SIF model the lower final B_s values predicted by their model (the DCC model) is due to the extra push on fluxoids **due** to F_n, which they believe is absent in the SIF model. As we have argued above the driving cause of the flux expulsion in all FBE models, including the DCC model, is however the combined force $F_b + F_c$ which results in the lower final field values in these models.

The above discussion highlights the possibly important role of buoyancy – should that concept be relevant ! – for the field decay in neutron stars. As already discussed, if *collective effects* dominate fluxoids motion then buoyancy will take a secondary role, and pinning force will, indeed, be the driving force causing flux expulsion.

3.3.2 FBE Models: various forces compared

Although the relative velocity of fluxoids and vortices, and hence the field evolution, behave very similarly in the different models the role of the different forces are different in the different FBE models. The combined force $F_b + F_c$ in the models A1, A2, and DCC is always positive (Fig. 3.4), as assumed, and is balanced by the drag force, F_v, in the earlier times ($t \lesssim 10^6$ yr) and by the pinning force in all later times. The **drag** force follows a behavior obviously same as the core field, and is negligible at late times

($\gtrsim 10^7$ yr) when B_c has achieved its final values. On the other hand, for the models B1, and B2 the force $F_b + F_c$ does become negative and restrict the flwoid velocity to remain smaller than the adopted maximum velocity $v_{max} \sim 3.2 \times 10^{-9}$ cm s^{-1}, for the assumed value of $\tau_{Ohm} = 10^7$ yr in Fig. 3.4. This happens during the forward creep phase for the B1 model due to the dominance of the positive F_n over the drag force F_v. In the B2 model, however, smaller value of $F_n << F_v$ requires $F_b + F_c$ to be positive during this phase.

Comparison between the results for models A1 and DCC in Fig. 3.4 reveals that the two models produce similar results in many aspect. Nevertheless the A1 model has the added advantage that the sharp jump in the value of $F_b + F_c$ for DCC has disappeared in the results of A1. On the other hand, in both cases the dominant force at early times are F_n and F_v which balance each other. At late times however F_n becomes negative and is balanced by $F_b + F_c$; the drag force F_v being negligible.

In model A2, F_n is estimated assuming a neutron vortex is infinitely rigid and hence remains straight throughout its length while creeping. As a consequence the push on the fluxoids due to the vortices at early times is much smaller (see **§ 3.3)** than for the A1 model. Fluxoids move much slower under this approximation than otherwise, and the drag force is balanced by $F_b + F_c$ instead of F_n in case of A1. The balance of forces at late times is however similar to that in A1, and DCC.

The role of F_v at early times, when fluxoids have the largest speed in model A1 is played in the B1 model by $F_b + F_c$ which can become negative in this case. Model B1 assumes same prescription for evaluation of F_n as in A1, but v_p is in this model restricted to remain smaller than a maximum value v_m where v_m = 3.2 x 10^{-9} cm s^{-1} for results in Fig. 3.4.

Finally, in the B2 model F_n is calculated as in A2 (assuming vortices remain straight while creeping), and $F_b + F_c$ as in B1 (assuming fluxoids are never bent thus their velocity cannot exceed the given maximum value). The time evolution of the forces as predicted in the B2 model are similar to that of A2 shown in Fig. 3.4. This is expected since the difference between the two models (B2 versus A2) is only for the restriction

$v_p \leq v_{max}$ assumed in the B2 model, which is however almost satisfied even in the A2 model. Thus the force $F_b + F_c$ never becomes negative in B2, although it does in B1, and remains positive and dominant over F_n while both are being balanced by F_v.

It was remarked earlier that models B1 & B2 may also be interpreted as representing the case for a drag force due to coherent scattering of electrons by the fluxoid lattice which inhibit the relative motion between the two. The flux expulsion is however still not prohibited since the two might move together, subject to a maximum velocity imposed by the boundary conditions on the motion of electrons. Any attempt to move the fluxoids at a larger velocity would be opposed by the large drag force which will adjust itself to cancel out the other existing forces.

Notice that for this interpretation of the results of models B1 & B2 however the lines in the force plots in Fig. 3.4 corresponding to $F_b + F_c$ (the *dotted line)* would now represent the viscous drag force if it is more negative than F_v (the *full line).* The similarity between force behavior for models B2 and A2, discussed above, shows that the drag force (due to coherent scattering) would be of no major consequence if F_n is calculated according to Eq. **3.7.** Namely rigid straight vortices would never try to push fluxoids at speeds larger than the assumed maximum velocity permitted by the core-crust boundary conditions for the accompanying motion of electrons with fluxoid lattice. On the other hand for the model B1 the new interpretation of the model renders its results similar to that of A1, as the *dotted line* in the corresponding plot for B1 in Fig. **3.4** has to be compared with the *full line* in the plot for A1. Thus in both cases the drag force is seen to be balanced by the outward directed pinning force which pushes the fluxoids at a velocity $v_p \sim v_{max}$ during early times, while at late times the negative pinning force cancels the force $F_b + F_c$.

To sum up the results of the different models presented in Fig. 3.4, the assumption of infinite rigidity of vortices which prevent each pinned segment of a vortex to creep independently than rest of the line have the effect of making the pinning force unimportant for the fluxoids motion. It thus reduces the flux expulsion rate only during early times ($\lesssim 10^6$ yr) of a pulsar lifetime. The opposing role of the pinning force

against fluxoids outward migration at late times ($\gtrsim 10^7$ yr) is however present in all the models. This is probably one or the characteristic feature common among all the FBE models discussed here. It is for this reason that in all of the models the field of a neutron star is prevented to decay to very small values ($< 10^8$ G) even after very long times ($\gtrsim 10^{10}$ yr). As already discussed, the FBE models share with the earlier studies (Muslimove & Tsygan 1985; Harvey et al. 1986) in having the buoyancy force (plus the outward directed tension force in case of DCC) as the driving cause of the flux expulsion out of the core of a neutron star. However, inclusion of the pinning force in these models (FBE) serves to regulate the rate of expulsion, and in particular to save a residual amount of flux ($\gtrsim 10^8$ G) for the star through its retarding force throughout most of the star's lifetime (ie. at $t \gtrsim 10^7$ yr).

3.3.3 Surface Fields

The evolutionary tracks for single pulsars on the B_s–P_s diagram as predicted in SIF and DCC (the latter being typical for all FBE models) are plotted in Fig. 3.6 for the different assumed initial field strengths. Points corresponding to the different ages of the neutron star are also marked along each track. As is seen in Fig. 3.6, the final strength of B_s as predicted in any of the FBE models is found to depend sensitively, and with an inverse proportionality, on the initial value of B_{s_i}. However the predicted final B_s is insensitive to the assumed initial values of P_s and B_c for changes in these quantities by almost two orders of magnitudes. This behavior may be also stated in a different way which is probably easier to grasp. The amount of flux expulsion is directly proportional to the initial value of B_{s_i}, which is expected because larger values of P_s are achieved for larger initial B_s values (see above). The final value of B_s according to the SIF model does however depend on the initial values of P_s, B_c, as well as that of B_s, even though with a direct proportionality in this case. These latter correlations are in accord with the assumed relation $\frac{\dot{B}_c}{B_c} = -\frac{\dot{P}_s}{P_s}$ in the SIF model, corresponding to $v_p = v_n$ at all times.

An observationally interesting point to note in Fig. 3.6 is that while according to

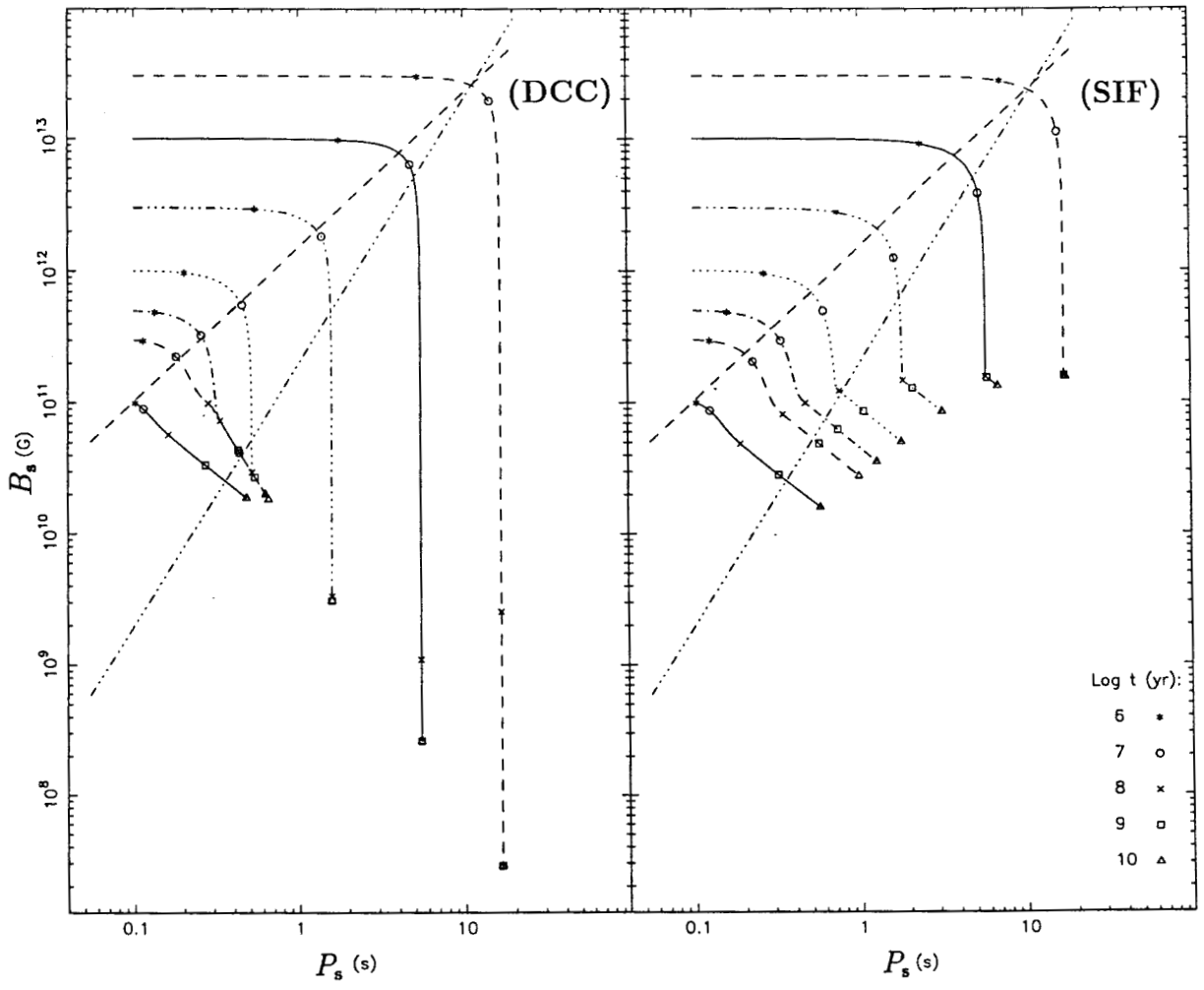

Figure 3.6- Surface field versus spin period evolution of solitary pulsars born with the different assumed initial field strengths, as predicted in the different models discussed in the text. The results shown are for the SIF and the DCC models while the latter is similar to those of the other FBE models. Positions of the neutron stars at various ages are marked on each track, and the spin-up line and the death line are also shown in each panel. A value of $\tau_{\rm Ohm} = 10^7$ yr has been used.

SIF very old neutron stars (ages $\sim 10^{10}$) are expected to have rather large magnetic fields in the range 3 x $10^{10} < B, < 2 \times 10^{11}$ G, the FBE models predict values of $B_s < 10^{10}$ G for these stars. An even smaller upper limit of $B, < 10^9$ G at ages > few x 10^8 yr is also implied by the results of FBE for neutron stars with initial field values of $B_s \gtrsim 10^{12}$ G. It has to be also noted that the results in Fig. 3.6 are derived for $\tau_{Ohm} = 10^7$ yr, and the predicted final fields would be smaller if larger values of τ_{Ohm} are used (compare Fig. 3.2a with Fig. 3.2b).

y-ray bursters :

The strengths of the magnetic fields of the very old neutron stars and their statistics are issues of relevance to the study of at least a sub-class of γ-ray burst sources which are likely to be highly magnetic old neutron stars (see eg. Blandford 1992). While such an identification of the γ-ray bursters does not seem to be consistent with the above predictions of FBE (represented by the results for the DCC model in Fig. 3.6) for the field strengths expected in old single neutron stars, could be however accommodated in the SIF model.

Ruderman & Cheng (1988) have proposed that the burst sources may be neutron stars with their magnetic axes aligned with their rotation axes. Ding et al. (1993) suggested that for an aligned neutron star the core field according to their model would not be expelled even on large time scales (>> 10^7 yr), unlike the general case presented in Fig. 3.6. Two crucial and doubtful assumptions have been however made to derive such a behavior for the case of an aligned pulsar. In spite of the assumed alignment of the surface dipole field with the rotation axis of the star fluxoids and vortices are still thought to be inclined to each other, or otherwise their entanglement being effective and the same pinning force as for the non-aligned case acting on fluxoids. Secondly, and even more serious is that the spin-down torque on a pulsar is considered to be only due to the magnetic dipole radiation which is thus diminished for an aligned case (Ding et al. 1993). This is in contrast to the general consensus that the rate of spin-down of solitary pulsars is apparently independent of the inclination angle; an idea

which is commonly adopted to infer the strength of the surface fields of pulsars (cf. Eq. 1.26 and Eq. 2.7). The spin-down rate for any given angle of inclination between the rotation and the magnetic axes of the star is believed to be the same as that due to the magnetic dipole radiation of a perpendicular rotator (Taylor & Manchester 1977; Srinivasan 1989). The theoretical rationale for this is the well-known Glodreich-Julian model (Glodreich & Julian 1969) according to which an *aligned* neutron star would act as a homopolar inductor capable of generating voltages $\sim 10^{16}$ volts. The charged particles are hence pulled out of the surface and those which are not trapped in the magnetosphere will flow out along the open field lines which extend beyond the light cylinder. The amount of angular momentum carried away by the escaping charged particles in the case of an aligned neutron star turns out to be comparable with that due to the emission of magnetic dipole radiation for a perpendicular case (Ostriker & Gunn 1969).

Therefore the assumption that the spin-down rate of an aligned neutron star would be negligibly small and its consequence for the field decay as inferred by Ding et al. (1993) has to be dismissed. Nevertheless, since a discussion of the predicted field decay by the FBE models for the *tentatively* assumed case of little spin-down torque acting on a neutron star serves to further elucidate the nature of the models we will discuss. Indeed, if the spin-down rate of a neutron star is assumed to be small the core field according to FBE models would not be expelled even on large time scales ($>> 10^7$ yr). This is because a reverse creep phase does not occur in this case since the required value of $|F_n(\omega = -\omega_{cr})|$ for a reverse creep phase to occur would be too large. The expected large value of F_n in this case is because of its inverse proportionality on P_s (see Eq. 3.5) and the expected small values of P_s due to the assumed small value of the spin-down torque. However, Ding et al. (1993, the last equation in their paper) argued that the large value of F_n in this case is a consequence of the dependence of ω_{cr} on B_c. This cannot be so because $|F_n(\omega = -\omega_{cr})| \propto 1/B_c^{\frac{1}{2}}$, which implies an smaller value for $|F_n(\omega = -\omega_{cr})|$ in this case. In fact the reverse creep phase starts always at a large value of B_c even in (the non-aligned) cases where a substantial field decay does

occur, as might be expected from the above dependence of F_n on B,. The difference in the predicted behavior of field decay for the present case is rather due to the fact that in this case P_s retains its assumed small initial value. This conclusion may be clearly verified by comparing the two cases of field evolution presented in Fig. 3.7. The two cases in Fig. 3.7 both are for an assumed very small spin-down torque (ie. that expected due to only dipole radiation for an inclination angle of 1 deg) but with different initial values for the spin period of the pulsar. Although in both cases B_c is large before the reverse creep phase, however substantial flux expulsion takes place in the case where P_s is large. Note that in this latter case the reverse creep phase starts from the very beginning and persists throughout the evolution of the star. This clearly verifies the effect mentioned above for P_s in determining the conditions for occurrence of a reverse creep phase.

Hence the identification of γ-ray bursters as old neutron stars having strong dipole magnetic fields would be consistent with predictions of the FBE models, provided they are not spun down to large periods $\gtrsim 1$ s. This conclusion is however independent of whether or not the surface field is aligned with the rotation axis of the star.

Active lifetimes of pulsars :

The active lifetimes of pulsar (defined in § 2.3) for the predicted spin-field evolution in the different FBE models are shown in Fig. 3.8 against the initial field strengths for values of $\tau_{Ohm} = 10^7$ and 10^8 yr, separately. Corresponding curves for the case of a purely exponential decay of the stellar magnetic field are also included, for comparison. Recall that in the latter case the total surface field is assumed to decay exponentially on the given time scale τ_{Ohm} with no constraint. The results of the different FBE models are very similar as can be seen in Fig. 3.8 (this is true for the A2 and B2 models also but they have been omitted for clarity). This is rather unfortunate as it renders any attempt to choose among them by comparing their predictions against the observed pulsar population hopeless. Nevertheless, the marked difference between the results of FBE and SIF in contrast to those of the exponential decay, in particular for values

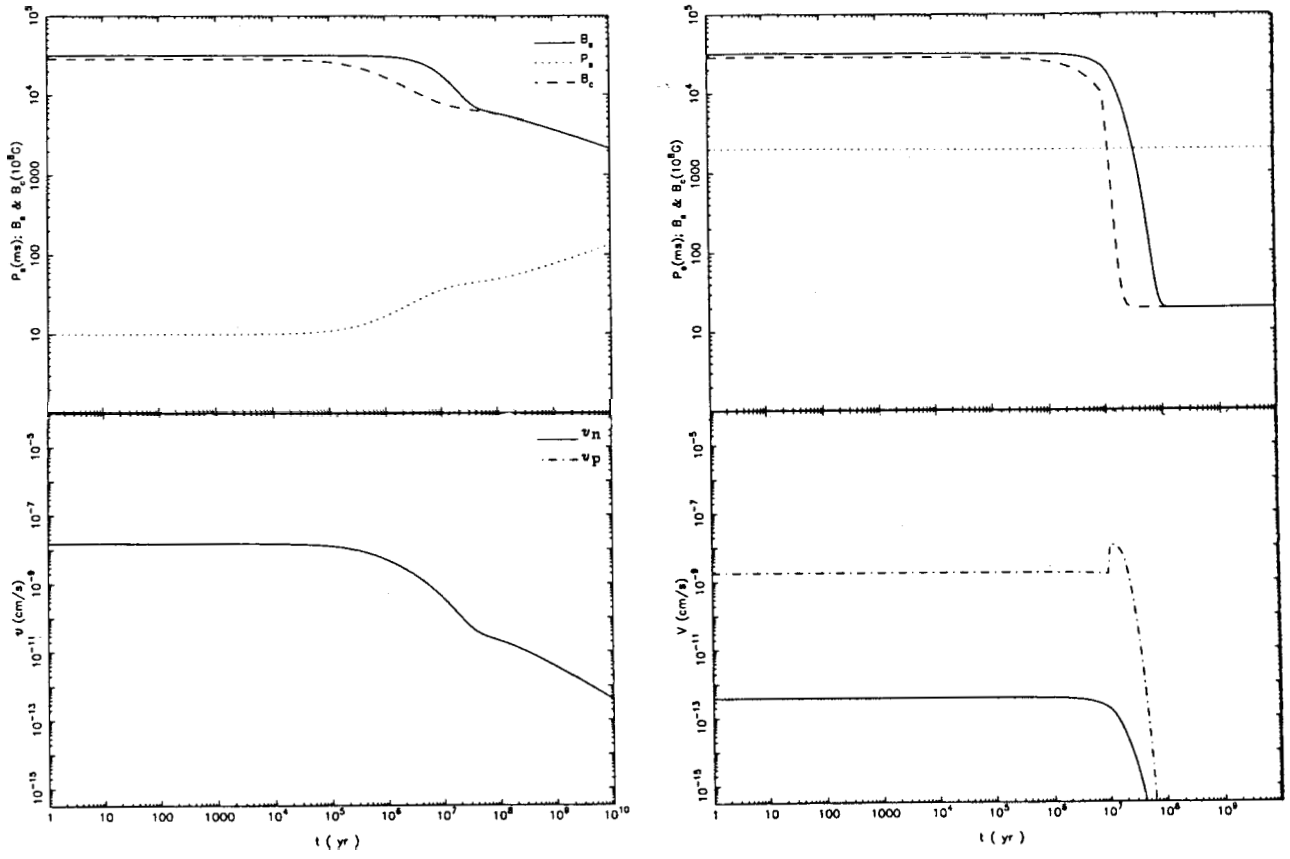

Figure **3.7**- The spin-magnetic field, and the velocity plots as in Fig. 3.2a and Fig. 3.1 but for a tentatively assumed case of a small spin-down torque (corresponding to the dipole radiation torque alone for a star with nearly parallel spin and megnetic axes) acting on the neutron star. The left two plots are for an initial value of the spin period $P_s = 0.01$ s, while the *right* plots are for the case with initial $P_s = 2.0$ s.

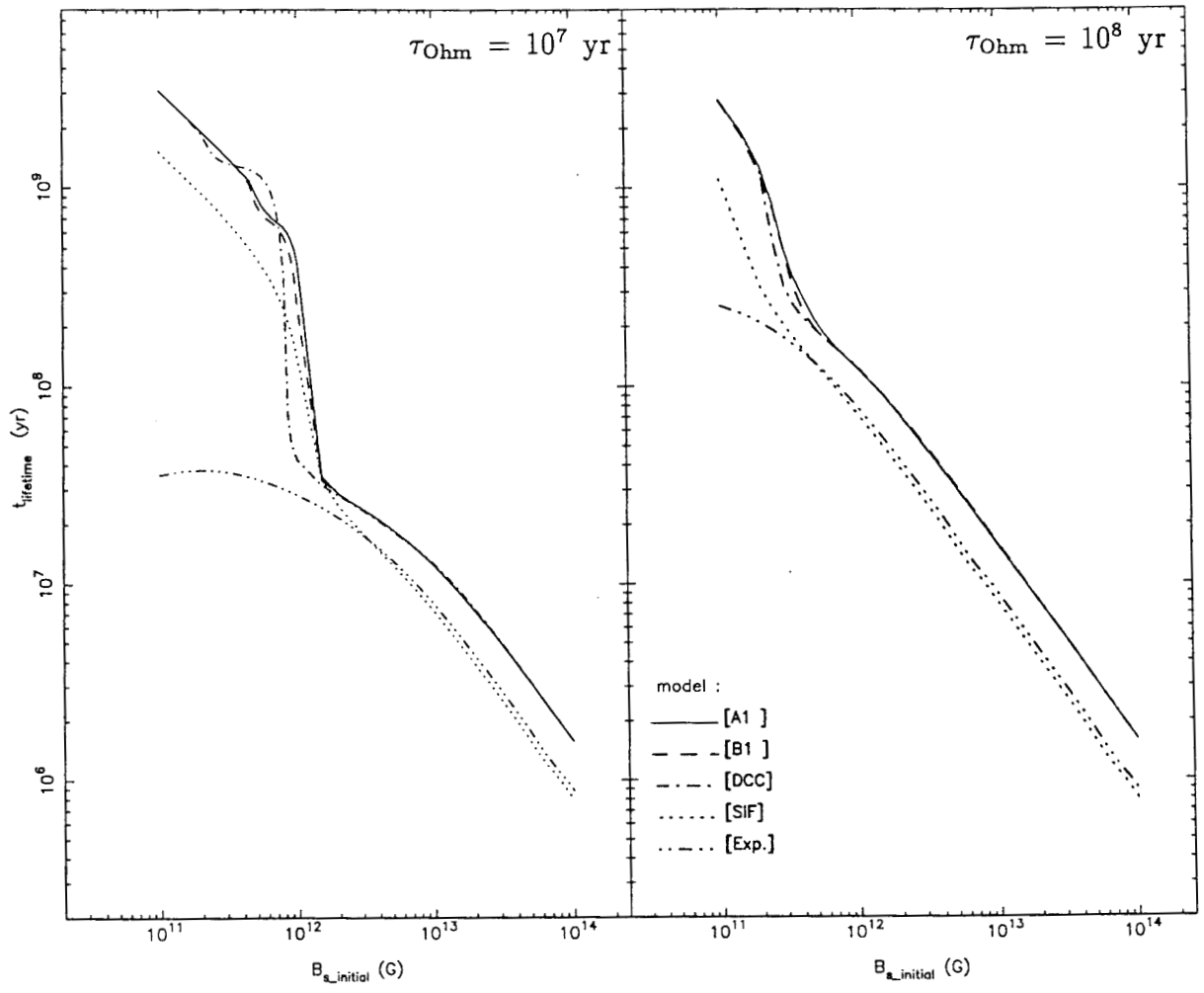

Figure **3.8**- Expected radio-active lifetimes of radio pulsars versus the initial surface fields, as predicted in the different field decay models represented by the different curves. Results for the two different values of τ_{Ohm} are shown in the two plots separately.

of $\tau_{Ohm} \lesssim 10^7$ yr, seems to furnish further support to the core-field expulsion scenario in general. This is because the much larger lifetimes predicted in these models (FBE and SIF) for pulsars with initial values of $B_s \lesssim 10^{12}$ G (Fig. **3.6)** seems to offer new insights into some of the problems with the statistics of pulsar population. Since the effect is exactly similar to that already discussed in chapter 2 for the results of the SIF model we refer to sections **§ 2.3.1** and **§ 2.3.2** for the observational consequences of the predicted increase in the lifetimes of pulsars.

3.4 Recycled Pulsars

As we saw in the earlier chapters the spin evolution of a neutron star in a binary system with a mainsequence star is expected to be quite different from that of a single pulsar. The interaction of the neutron star magnetosphere with the stellar wind of the companion star is believed to result in large values of $P_s \sim 10^4 - 10^5$ s, in contrast to the much smaller values achieved in the case of single pulsars. Prediction of any of the field expulsion models (FBE and SIF) for the magnetic evolution of binary neutron stars are therefore expected to be in principle different than for the single stars. In fact, simulations of the spin and magnetic evolution of binary pulsars based on SIF have been already shown to reproduce the observed properties of the recycled pulsars in low-mass binaries, as noted in chapter 2. In this section we apply the FBE models for the first time to neutron stars in binaries. In order to extend the results of the FBE models to the case of binary evolution of neutron stars, we have adopted a similar prescription for the spin evolution of a neutron star in a binary system as that in chapter **2.** The computations were repeated, in the case of each of the FBE models, for the different combinations of the following values of the parameters and initial conditions:

$P_{\rm orb}$: 2 – 600	(day)
ξ: 1, 10, 100	
$\log \tau_{\rm Ohm}$: 7.0, 8.0, 9.0	(yr)
1 M: −15, −14, −13	($M_\odot$/yr)
initial $P_{\rm s}$: 0.1, 1.0	(s)
initial B,: 3×10^{12}	(G)
initial $B_{\rm c}$: 2.7×10^{12}	(G)

where $P_{\rm orb}$ is the binary orbital period, M is the mass-loss rate of the companion star, and ξ is a scaling factor for the rate of the angular momentum transferred out of a neutron star in a spin-down phase. A value of $\xi = 1$ corresponds to that due to the difference between the Keplerian and the co-rotation velocities at the magnetospheric radius. Larger values of ξ associated with a more effective loss mechanism might be expected for assumptions different from those adopted (eg. a spherical rather than the disc-like geometry assumed for the accretion flow, etc.; see § 1.3 for details). A spin-up phase of the star is assumed to have no further effect on its magnetic evolution, and the core field is kept constant during such a period of time. The evolution of a neutron star in a binary with a low-mass companion (of a mass M = 1.0 $M_\odot$) is followed for a period of 10^{10} yr, and its final surface field as predicted in each of the field decay models has been determined, for different combinations of the parameter values.

The predicted distribution of the final field strengths versus initial orbital periods are plotted in Fig. 3.9. The results due to the different FBE models are found to be similar in many cases; however large differences are also observed in some cases. The observed low-mass binary pulsars with existing estimates for their field strengths and orbital periods are again compared with the model predictions (as we did for the SIF model in chapter 2, in Fig. 2.8 and Fig. 2.9). Data on 8 binary pulsars which are expected to have been recycled in low-mass binary systems are presented in Fig. 3.9 (cf. Table 2.1). The observed orbital periods in these systems have been corrected for the expected change in the orbital period during a final Roche-lobe overflow mass transfer phase as indicated in Table 2.1. Within the uncertainties associated with the

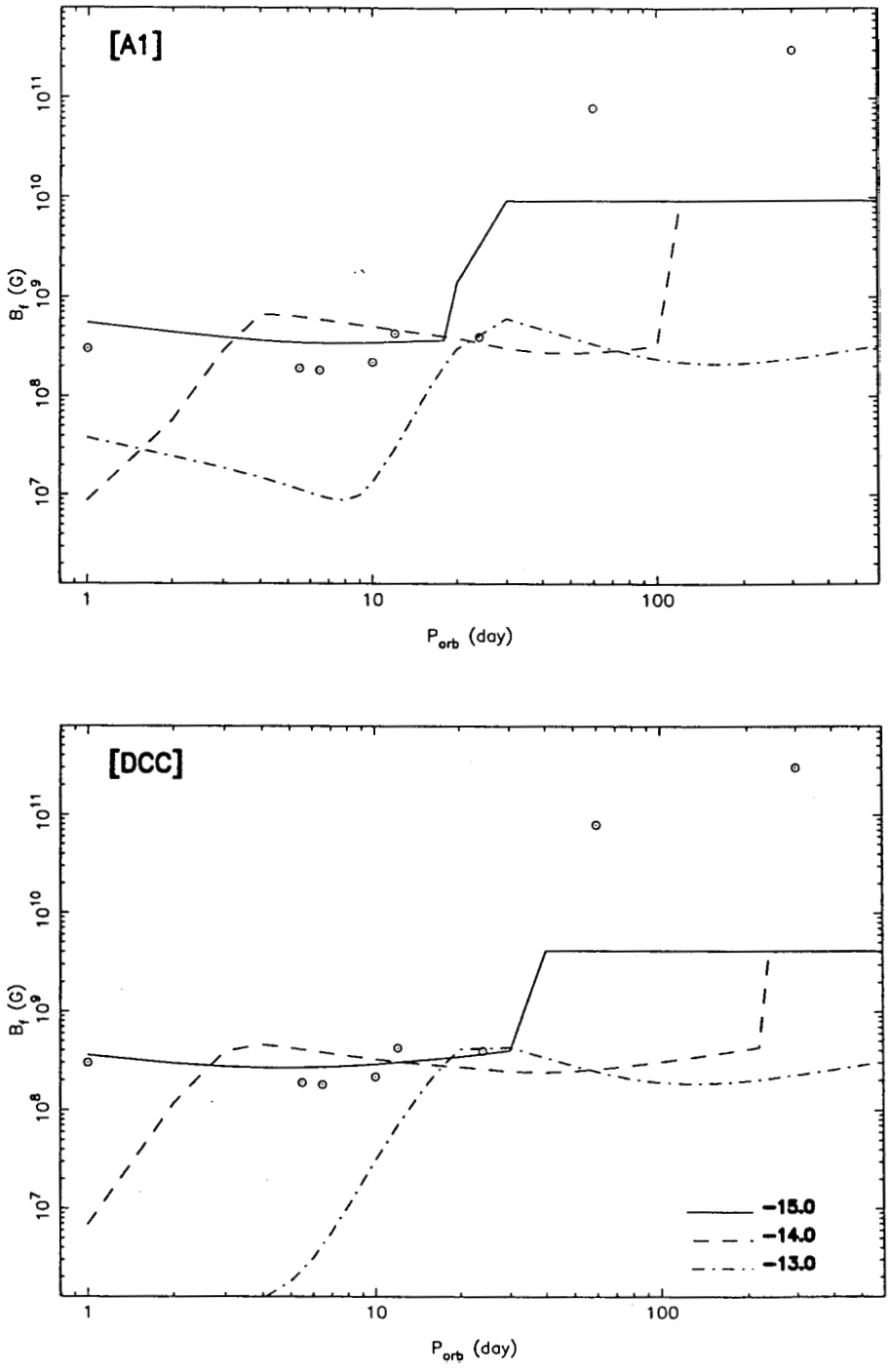

Figure 3.9- Final values of the surface magnetic field strengths of neutron stars evolved in low-mass binaries with different orbital periods, as predicted in the FBE models. The other models (namely A2, B1, and B2) also produce similar results. Predictions for the different assumed values of the companion mass-loss rate $\dot{M}_2$ (in units of $M_\odot/\mathrm{yr}$) are indicated by the different curves. Encircled dots represent observed binary radio pulsars that are descendants of wide low-mass binaries, for which the initial orbital periods can be estimated. Initial values of $B_s = 3.16 \times 10^{12}$ G, $B_c = 2.85 \times 10^{12}$ G, and $P = 0.1$ s have been assumed. Values of $\tau_{\mathrm{Ohm}} = 10^7$ yr and $\xi = 10$ have been used.

value of M which could be, as well, varying with time and also have a dependence on the orbital period in the case of close orbits the computed curves in Fig. 3.9 seem to agree with the observed data. As was discussed in chapter 2 for the case of SIF, one has also to take into consideration the dependence of the results on the various other parameters (namely initial spin period and field strength of the neutron star, companion star's wind velocity, efficiency of the imparted torque on the neutron star during spin-down phase, and the unknown decay time scale of the field in the crust) while judging the success of the models. Qualitatively similar results are produced for many other choices of the parameters values different than those in Fig. 3.9 (and also by the other FBE models namely A2, B1, and B2 which are not shown). Comparing the predictions of the FBE models for the final field strengths of neutron stars recycled in low-mass binaries with those of the SIF model discussed in chapter 2 we find larger values of $\tau_{\rm Ohm}$ and/or larger values of ξ are preferred by the SIF model as compared to the FBE models, for the same given initial values of B_s, B_c, and P_s. We recall that, the results in chapter 2 showed that values of $\tau_{\rm Ohm} \lesssim 10^9$ yr together with $\xi \lesssim 1$, or $\tau_{\rm Ohm} \gtrsim 10^7$ yr together with $\xi \gtrsim 10$ were preferred by SIF as far as the data on the low-mass systems were concerned.

Nevertheless, the diverse values of the final field strengths in each of the panels in Fig. 3.9 clearly show the dependence of the predicted field evolution of binary pulsars on their orbital evolution: for the same initial spin period, core and surface field strengths, and the crustal decay time scale, the predicted *unique value* for the final field of a *single* neutron star is to be contrasted with the *largely different* final values obtained in binaries, seen in Fig. 3.9 along each curve and among the different curves in each plot. In addition to the dependence on orbital period and mass-accretion rate demonstrated by the plots in Fig. 3.9 the field evolution of binary pulsars as predicted in FBE models is found to depend also on the other parameters (see above) as well. Hence, as remarked earlier one may not apply the results for the solitary pulsars to those evolved in binaries.

As discussed earlier, the pinning force on fluxoids acts as an obstacle against an otherwise more rapid and enhanced flux expulsion out of the core of solitary pulsars.

The same is true for neutron stars evolved in many of the assumed binary systems which we have tested. This may be verified again by comparing between the predicted field evolution for a binary neutron star according to the FBE models (say the DCC model) with what is expected if $F_b + F_c = 0$ as we did for the case of solitary pulsars in Fig. 3.5. In Figs 3.10a the predicted evolution of spin-magnetic fields according to DCC for a neutron star in a binary with $P_{orb} = 20$ day are contrasted with that expected for the same binary if the pinning force were the only driving force present, namely assuming $F_b + F_c = 0$. Fig. 3.10a shows that setting $F_b + F_c = 0$ result in a much smaller flux expulsion than otherwise. This, in addition to the fact that in the absence of F_n all of the flux would be expelled (see § 3.3) proves the braking role of F_f.

Comparing between Fig. 3.10a and Fig. 3.5b the results for the case of setting $F_b + F_c = 0$ are seen to be similar. This might imply that if the pinning force were to be considered as the only existing cause for the flux expulsion (namely $F_b + F_c = 0$) then field evolution of neutron stars recycled in binaries would be same as that of the single stars and their fields would never decay by more than an order of magnitude. This is not so. Fig. 3.10b is similar to Fig. 3.10a except that for the orbital period $P_{orb} = 120$ day. In Fig. 3.10b the field is seen to decay *due to the pinning force alone* down to a value $\sim 10^{10}$ G from its initial value $10^{12.5}$ G. The binaries for which such an expulsion of core flux by the pinning force might occur are those of an intermediate orbital periods depending on the values of the other parameters. In wider orbits an effective spin-down would not occur and hence the essential fast outward motion of vortices accompanied by the fluxoids is not realized. In the very tight orbits on the other hand the spin-down of the neutron star to very large periods does not allow the fluxoids to be pulled out along with the vortices during the spin-down phase (notice the much smaller values of the fluxoid velocity, v_p, than that of vortices, v, during the late spin-down phase at times $\gtrsim 10^9$ yr in the results for the case with $F_b + F_c = 0$ in Fig. 3.10a). Namely a *co-moving* state of flwoid-vortex motion during the spin-down phase which is realized for the wider orbits (as in Fig. 3.10b) is not possible due to the inverse dependence of the fluxoids velocity on P_s discussed earlier in § 3.3 (see

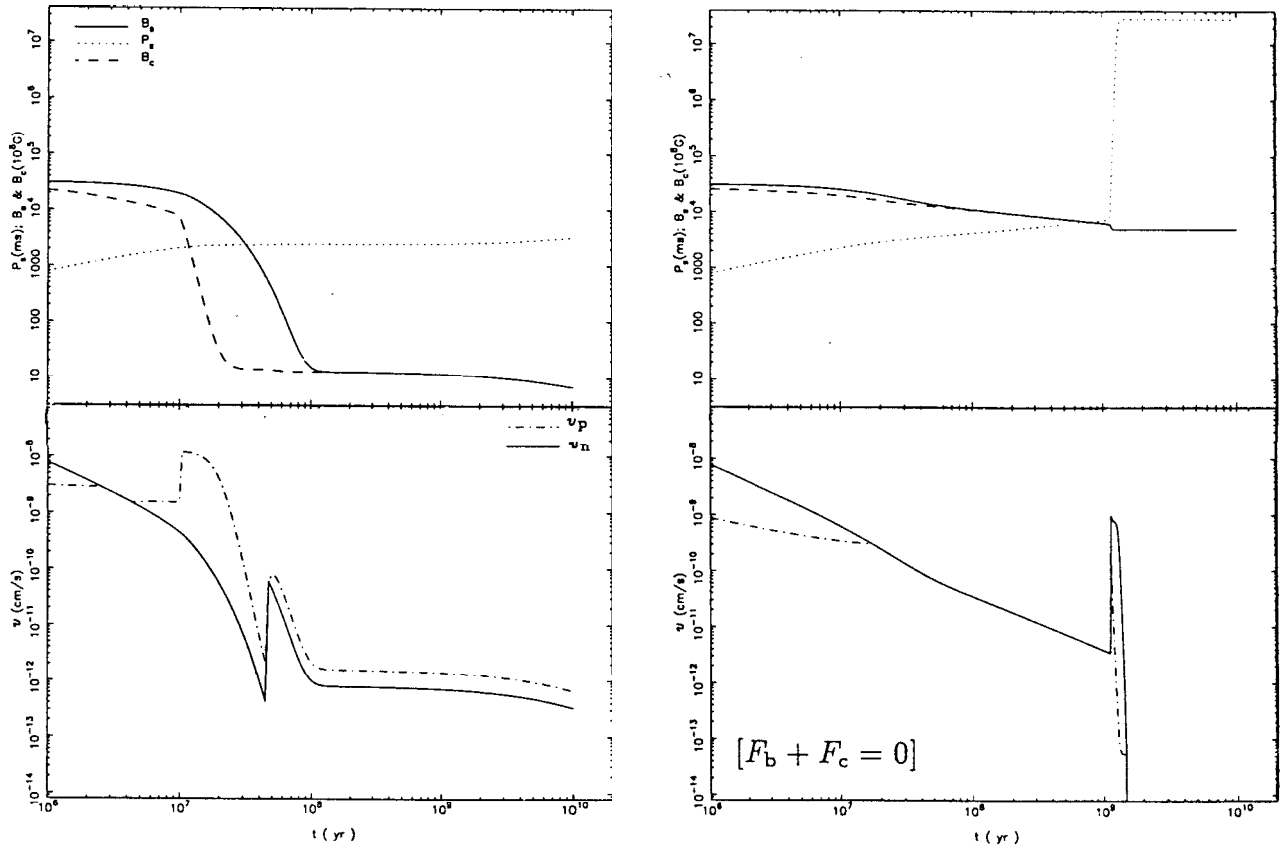

Figure 3.10(a)- The left two panels show the spin-magnetic field, and the vortex-fluxoid velocity evolution for a neutron star in a binary with a 1 $M_\odot$ companion star and an orbital period $P_{orb} = 20$ days. The results for the assumed case of $F_b + F_c = 0$ throughout the evolution of the star for the same binary and initial conditions are shown at the right. Initial values of $B_s = 3.16 \times 10^{12}$ G, $B_c = 2.85 \times 10^{12}$ G, and $P_s = 0.01$ s have been assumed. Also values of $\dot{M}_2 = 10^{-14}$ $M_\odot$/yr, $\tau_{Ohm} = 10^7$ yr, and $\xi = 10$ have been used.

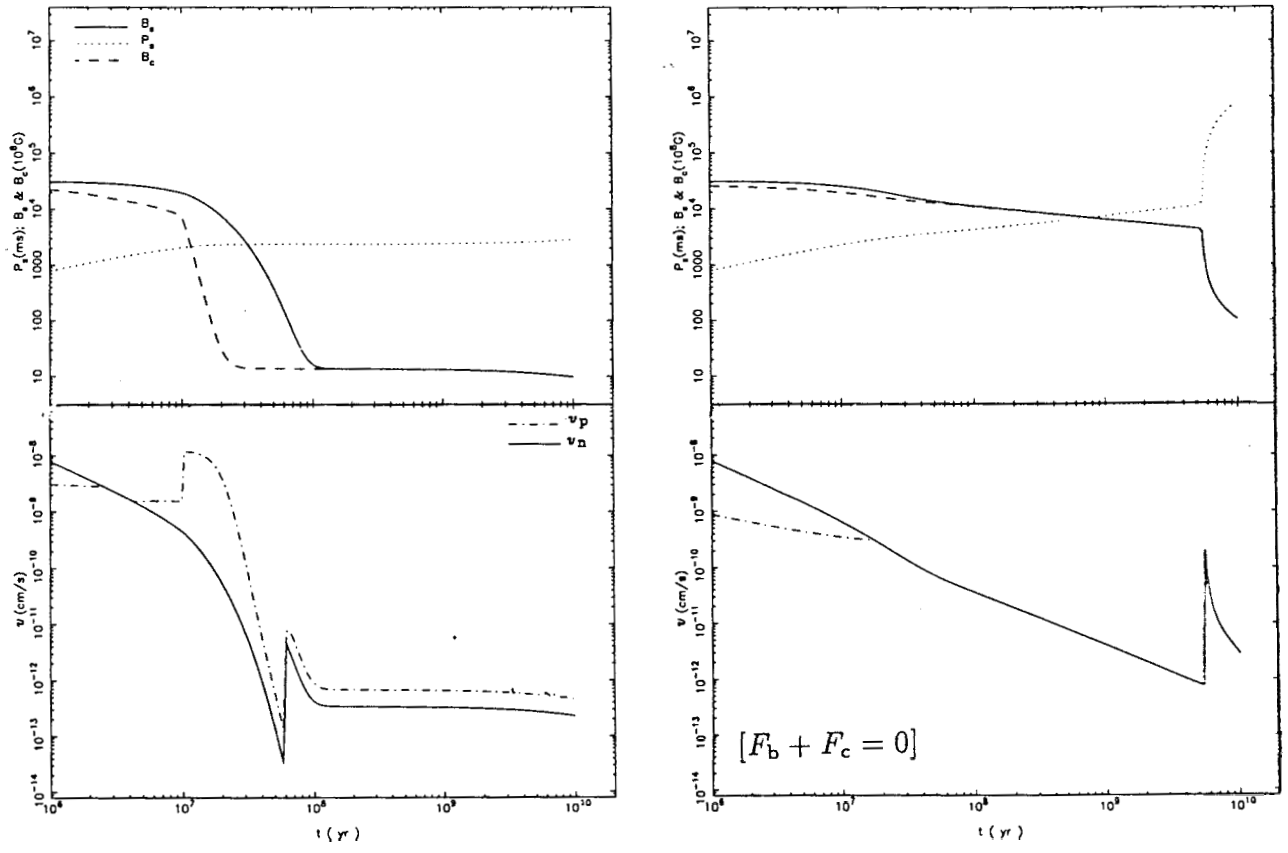

Figure 3.10(b)- Same as Fig. 3.10a, but for the case of a binary with $P_{orb} = 120$ days.

also Eq. 3.5). This dependence is understood as the larger spin periods means larger inter-vortex separation and hence smaller pinning force per unit length of the fluxoids.

Notice that in the absence of $F_b + F_c$ the two binaries (with $P_{orb} = 20$ and 120 days) are predicted (Fig. 3.10a versus Fig. 3.10b) to result in different values for the final field strengths. However this difference is washed out in the FBE models by the dominant role of $F_b + F_c$ over F_n, and the final field values are similar for the two cases shown in Figs 3.10a & b. Although the case in Fig. 3.10b is not sufficient to explain field values as low as that of millisecond pulsars by a model which discards the buoyancy force (in presence of the assumed viscous drag force) the possibility of such a model does not seem to be ruled out. However, as remarked earlier the role of the pinning force which was argued above to be one against the expulsion of the flux driven by the buoyancy force is essential to stop the field decay in binary neutron stars at values comparable to those observed in old recycled pulsars. *In other words the possibility of a model which discards the pinning force and relies only on the buoyancy* is *absolutely ruled out.* Thus, while the pinning between fluxoids and vortices provides a means for explaining the residual fields of old binary and millisecond pulsars, it also serves to establish a dependence between the final field of the star and its spin period history driven by interaction with matter accreted from its binary companion.

3.5 Main conclusions of the chapter

In the second chapter we explored the scenario of spindown-induced flux expulsion model (SIF model). In that model – in which the flux expulsion occurs due to the interpinning of the vortices and the fluxoids – it was explicitly assumed that the flwoids will move with the *same velocity* as the vortices. The outward velocity of the vortices is, of course, determined by the spindown rate of the neutron star. This led to the conclusion that in the case of a neutron star in a binary system very low fields can be attained due to the dramatic flux expulsion during the stellar wind phase of the companion.

In this chapter we have tried to improve upon the SIF model by including not only the pinning force on the flwoids but also the viscous drag force on it due to electron scattering, possible buoyancy force acting on the fluxoids, and also curvature force on the fluxoids should their geometry deviate very linearity. In previous sections we have systematically presented the results obtained. In all this, of course, *it has been assumed that the fluxoids move independently of one another.* Within this assumption we have explored several variations of the theme. For example, in one of the models the vortex is assumed to remain straight as it creeps outwards. In an alternative model each segment of the vortices between successive pinning centres is allowed to move independently. For the sake of convenience we would like to briefly summarize some of the more significant results and conclusions obtained in this chapter.

- The main consequence of the inclusion of the drag forces on the vortices is that in the early phase of evolution – when the spindown rate is quite large – the fluxoids are not able to keep up with the vortices. In other words, unlike in chapter 2 one encounters a phase where the velocity of the fluxoids is *less* than the outwards velocity of the vortices.

- But eventually, as the vortices slow down they are able to drag the fluxoids with them. It is during this co-moving phase that a substantial fraction of the flux expulsion occurs.

- In the later phase buoyancy force becomes the dominant one. If this concept of buoyancy is relevant (at the moment this is a controversial point) then it leads to a situation where the fluxoids lead the vortices. As discussed earlier, there has been a suggestion in the literature that the magnetic field decay can be explained solely in terms of buoyancy of the fluxoids and the consequent outward migration. We would like to forcefully argue that this cannot be so. Even if buoyancy is relevant, one cannot do away with the role of the pinning force. Quite simply, if pinning force is not present then buoyancy will result in vanishing field strengths for very old pulsars, in particular the millisecond pulsars. In the models we have discussed in this chapter we have been able to obtain reasonable field strengths for recycled pulsars, including the millisecond pulsars – this in spite of the inclusion of the buoyancy – because interpinning of fluxoids and vortices makes buoyancy less effective. *Pinning force acts as a brake.*

- In our opinion this provides the strongest argument for pinning interaction between fluxoids and vortices. In the absence of it the only way to explain the decay of the magnetic field trapped in the core of the star is to invoke buoyancy. Unfortunately, while buoyancy is admittedly a possible mechanism of flux expulsion it is *too effective!* The only way one can understand the observed low but significant fields of millisecond pulsars is by invoking the pinning force. Either the pinning alone does the job (viz., the vortices drag the fluxoids) or pinning reduces the efficacy of the buoyancy force. *Either way pinning is an essential ingredient. We feel that this is one of the most significant conclusions of this chapter.*

- We explored four different models in this chapter with the hope that we will be able to discern the relative importance of the various forces acting on the fluxoids. Unfortunately this was not possible since all the models produce more or less the same results. There are some differences, but given various uncertainties we would not like to draw any conclusions from them. Some general

statements can however be made.

The model where the vortices are assumed to be infinitely rigid dismisses the possibility of different segments of a vortex to move independently of the other segments. This in effect reduces the role of the pinning force. The common feature of all the models is the role of the pinning force in making the outward migration of the fluxoid less efficient at late times greater than $\sim 10^7$ yr. At these late times the role of the buoyancy would have been more significant had it not been for the pinning force.

- Having explored various models we are eventually led to the conclusion that the simple SIF model which assumes that the fluxoids and vortices move with the same velocity is not so bad after all! This is because much of the flux expulsion occurs during the co-moving phase.

- Having discussed various forces acting on the fluxoids we are left to conclude that the force whose inclusion makes a significant difference to the results obtained in the previous chapter is the drag *force.* Consider neutron stars with binary companions. In chapter 2 in which we had ignored the drag force there was a dramatic flux expulsion during the propeller phase when the neutron star was dramatically spun down. This is because there was no limitation to the velocity with which the fluxoids could migrate – they could move as fast as the vortices are able to move. The inclusion of the drag force significantly alters the conclusion. Since the flux velocity is limited by the drag force, the flux expulsion during the propeller phase is far less effective. The situation is very similar to the very early phase in the life of a pulsar when its spindown rate is so much that the fluxoids lag behind them.

- *Collective effects*: As already remarked earlier, in this chapter, like in the previous one, we have assumed that the fluxoids can move independently of each other (although one of the models we have explored mimics collective effects). Although there is no consensus as yet it is quite likely that collective rigidity of

the flux lattice as a whole may be profoundly important. Such collective rigidity arises due to coherent scattering of the electrons. Quite simply, a classical orbit of an electron will encompass a very large number of fluxoids. Therefore one may have to consider motion of not single fluxoids but large *bundles* of fluxoids. According to M.Ruderman (unpublished remarks), the force acting on N fluxoids moving together may be very much larger than N times the drag force on a single fluxoid. The arguments are very similar to the classical arguments for *flux freezing* in a conductor. If this is indeed so then it is very hard to understand how the magnetic flux can be expelled from the superconductor at all. This is a question that obviously requires very careful study, and we have nothing concrete to suggest at this stage.